ISPRS Journal of Photogrammetry and Remote Sensing 208 (2024) 121–135

Contents lists available at ScienceDirect

ISPRS Journal of Photogrammetry and Remote Sensing

journal homepage: www.elsevier.com/locate/isprsjprs

Landsat assessment of variable spectral recovery linked to post-fire forest structure in dry sub-boreal forests

Sarah M. Smith-Tripp [a,*], Nicholas C. Coops [a], Christopher Mulverhill [a], Joanne C. White [b], Jodi Axelson [c]

[a] Faculty of Forestry, University of British Columbia, 2424 Main Mall, Vancouver BC, Canada
[b] Canadian Forest Service, (Pacific Forestry Centre), Natural Resources Canada, 506 West Burnside Road, Victoria, BC V8Z 1M5, Canada
[c] Forest Science, Planning and Practices Branch, British Columbia Ministry of Forests, Victoria, BC, Canada

ARTICLE INFO

Keywords:
Forest disturbances
Forest structure
Lidar
Remotely piloted aircraft (RPA)
Satellite imagery
Spectral clustering

ABSTRACT

Forest disturbances such as wildfires can dramatically alter forest structure and composition, increasing the likelihood of ecosystem changes. Up-to-date and accurate measures of post-disturbance forest recovery in managed forests are critical, particularly for silvicultural planning. Measuring the live and dead vegetation post-fire is challenging because areas impacted by wildfire may be remote, difficult to access, and/or dangerous to survey. The difficulties of post-fire monitoring are compounded by the global increase in the frequency and severity of disturbances, as expansion of disturbed areas also increases the number and size of areas requiring post-disturbance monitoring. Methods that safely, efficiently, and extensively differentiate silviculturally beneficial coniferous growth from barren ground or deciduous shrubs are necessary to inform post-fire forest management. Satellite imagery can detect burn patterns, but monitoring changes in forest structure post fire is challenging due to complex vegetation responses. To overcome this challenge, this study combines post-disturbance spectral trajectory measures from a time series of historical Landsat imagery with field and remotely piloted aircraft (RPA) lidar (light detection and ranging) data to examine vegetation recovery of lodgepole pine (*Pinus contorta*) dominated sub-boreal forests after high-severity fires in 2006 in central British Columbia, Canada. Distinct spectral recovery trajectories were identified using data-clustering from a combination of seven Landsat spectral indices, with trajectories varying by recovery magnitude and rate. The forest structure associated with each distinct trajectory of spectral recovery was analyzed using 430 ha of spatially explicit forest structure measures (e.g., basal area, stem counts) and composition (e.g., percent coniferous) derived from 26 coincident field plots and high density RPA lidar (>200 points/m^2) data. By comparing spectral trajectories to forest structure measures, we found the most spatially abundant cluster of spectral recovery coincided with a basal area of 0.62 m^2/ha, high stem densities (>5000 stems/ha) and a high abundance of coniferous trees (>95 % coniferous). Around 10 % of the landscape was associated with relatively high abundance of deciduous vegetation (>20 %) in addition to very high conifer stem densities (>8000 stems/ha). By identifying the structural characteristics associated with unique Landsat spectral trajectories, we highlight the combined value of RPA lidar data and satellite image time series in providing a detailed and spatially explicit characterization of post-fire recovery relevant to managed forests.

1. Introduction

Wildfires are a ubiquitous global forest disturbance, particularly in the forests of dry interior western North America. In Canada from the 1980s to present, wildfires burned 2.5 times more land area than was harvested nationally (White et al., 2017a). Wildfires are expected to increase in size and severity as global temperatures rise and summers become drier and more prolonged, ultimately increasing the probability of ignition and fire spread (Baltzer et al., 2021; Pausas and Keeley, 2021; Westerling et al., 2006). Research demonstrates that increasing wildfire activity and changing climate shift the pathways of forest recovery, rearranging composition, and altering forest structures (Hansen and Turner, 2019; Stevens-Rumann and Morgan, 2019). Possible ecosystem recovery pathways can be characterized as quadripartite; as described

* Corresponding author.
E-mail address: Sarahsmith.tripp@alumni.ubc.ca (S.M. Smith-Tripp).

https://doi.org/10.1016/j.isprsjprs.2024.01.008
Received 26 May 2023; Received in revised form 18 December 2023; Accepted 12 January 2024
Available online 18 January 2024

by Seidl and Turner (2022), the four possible ecosystem pathways are: (1) no changes in forest composition or structure (forest resilience), (2) changes in forest structure (forest restructuring), (3) changes in composition (forest reassembly), and, (4) changes in both structure and composition (forest replacement). Which of these pathways is considered "ideal" or "desirable" for a specific forest depends on the ecosystem services provided by that forest (Millar and Stephenson, 2015) and the definition of post-fire ecosystem recovery (Bartels et al., 2016). If timber harvesting is a primary objective of forest management, measurements that quantify recovery of commercially important tree species are important. Thus, metrics of stand structure, such as basal area (BA), tree density (stems per hectare), and forest composition, including the ratio of coniferous to deciduous trees, should be prioritized when assessing potential silviculturally relevant recovery pathways (British Columbia Ministry of Forests, 2022).

After a stand-replacing fire, forests regenerate in two key phases (1) establishment and regeneration (3–5 years) followed by (2) young forest regrowth (10–20 years; Bartels et al., 2016). The young forest regrowth phase is a critical time to assess the successful growth of coniferous forest structure and composition. Differences at this stage may signal that a forest is not resilient and is following a recovery pathway that leads to stand restructuring (e.g. decreases in forest density) and/or reassembly (e.g. a shift in coniferous proportion: Seidl and Turner, 2022). In Canada, recent literature reviews have highlighted that natural disturbance research is relatively unrepresented in current Canadian forest research and monitoring, but such work is pivotal for effective ecosystem monitoring (Waldron et al., 2023). To mitigate the impacts of climate change, forest managers must take proactive steps to identify forests vulnerable to novel ecosystem change, including forests that may not return the desired stand composition or stocking density (Williamson et al., 2019).

Quantifying recovery after wildfire is important, yet recovery assessment in-situ is challenging, as deadwood often creates dangerous working conditions (Rakochy and Hawkins, 2006). The problem of recovery monitoring is compounded by the expansion of post-fire landscapes in western North America, where regenerating stands may be growing under different climate conditions than historic forests, impacting overall forest resilience (Davis et al., 2019). Historically, post-fire monitoring relied heavily on ground-based surveys, but the spatial extent of recent wildfires across much of western North America makes this approach impractical and prohibitively expensive (de Almeida et al., 2020). Spatiotemporally explicit and consistent sources of information are therefore needed to successfully characterize the possible pathways of forest recovery. This level of detail can be provided with data from satellite missions such as Landsat, which serves to capture recovery at broad spatial and temporal scales (Wulder et al., 2022).

Landsat is the most temporally continuous satellite mission; providing nearly half a century of spectrally consistent medium resolution (30 m) data at a global scale (Wulder et al., 2022; Young et al., 2017).The utility of Landsat and other satellite data for forest monitoring of burn-severity and remaining forest structure post-fire has been well-established. Remote sensing derived metrics of severity, such as the difference in the normalized burn ratio (dNBR), strongly correlate with in-field measures of burn severity (Chen et al., 2011; Miller and Thode, 2007). While differences in disturbance severity can describe post-disturbance forest structures (e.g., tree density; Cocke et al., 2005), severity metrics are influenced by prior ecosystem events (Harvey et al., 2019) and are not indicative of ecosystem recovery (Keeley, 2009). Other approaches, like the use of radiative transfer models or spectral mixture models can also be used to characterize post-disturbance recovery. However, radiative transfer models often require extensive parameterization for meaningful inference (Fernández-Guisuraga et al., 2021; Solans Vila and Barbosa, 2010), and spectral-mixture models require additional assumptions on what comprises a spectral end-member (Lewis et al., 2017). Nonetheless, such approaches have been used to characterize short-term recovery, particularly under varying burn severity conditions (e.g. Fernández-Guisuraga et al., 2021; Fernandez-Manso et al., 2016). Satellite-based measures of ecosystem recovery should include a suite of metrics such as stem densities or biomass, among others.

Modeling the relationship between satellite based spectral observations and structural measures is difficult for two main reasons. First, rapid ingrowth of mostly deciduous vegetation can mask coniferous recovery (Vanderhoof and Hawbaker, 2018). To overcome the issue of deciduous ingrowth, recent work suggests that incorporating multiple spectral indices (i.e. combining indices like the Tasseled Cap (TC) measures with NBR) may better explain landscape dynamics (Cohen et al., 2020). Combinations of spectral indices have been used to update stand-level inventories for mature forest structures (Bolton et al., 2018), yet, of these multi-index models, there has been little focus on capturing measures of early forest recovery – particularly relevant to silviculture. Spectral-mixture models also avoid index saturation and limit background effects (Adams et al., 1995). While they present a viable post-disturbance monitoring solution, past research does not capture a suite of silvicultural metrics, particularly forest structure metrics (Fernandez-Manso et al., 2016). In this case, spectral-mixture models do not make sense for modeling structural metrics such as basal area or stem density because there is no clear spectral 'end-member'.

A secondary issue for assessing forest structure as observed via satellite is that building these relationships relies on accurate forest structure measurements over large areas (White et al., 2022). One approach to gather accurate forest structure data over large areas is to combine satellite observations with comprehensive structural forest assessments from Lidar (White et al., 2017a; Coops et al., 2021). Lidar (light detection and ranging) offers a viable sampling technology for structural recovery assessment (Wulder et al., 2012). Lidar captures overstory structure, which drives satellite spectral responses, and penetrates through this overstory to describe below-canopy forest structure (Chisholm et al., 2013; Jarron et al., 2020). Additionally, the development of Remotely Piloted Aircraft (RPA) lidar systems offers a range of new benefits (Goodbody et al., 2017), like rapid sampling in diverse locations and descriptions of fine-scale vegetation, such as tree seedlings, at submeter accuracies (Shrestha et al., 2021). Spatially exhaustive RPA datasets, combined with field measures, can be used to generate wall-to-wall estimates of silviculturally relevant characteristics, including basal area and stem counts. With these metrics, we improve our capacity to measure forests recovering from disturbances at the meter resolutions required by forest managers (Moe et al., 2020).

Landsat is an important tool to assess forest recovery in the forest regrowth phase over large spatial scales (Wulder et al., 2009). Linkages between Landsat spectral observations of recovery and forest structural development in regenerating forests have been explored using field plot (White et al., 2023, 2019) and airborne lidar data (Chirici et al., 2020; Senf et al., 2019; White et al., 2018). However, less research has been undertaken to assess silviculturally focused metrics of recovery in relation to satellite spectra. Further, given the expanding extent of wildfire areas, the use of cost efficient RPA Lidar data datasets offers an opportunity to provide 'ground-truthing' data for spectral relationships (Pajares, 2015).

This paper explores how Landsat time series data can inform the spatially variable return of forest structure following a wildfire event. Our objective was to determine whether distinct expressions of forest structure, particularly expressions important for silviculture, are discernible using temporal trajectories of spectral indices in locations of high burn severity. We focused on silviculturally relevant structural recovery metrics that are of interest to forest managers, including: basal area, stem counts, and species composition. Of these metrics, we hypothesized that differences in composition would have the strongest differences in spectral trajectories, as deciduous trees are spectrally distinct from conifers and deciduous forbs are generally the fastest to recover (Vanderhoof and Hawbaker, 2018). We evaluated the relationship between Landsat spectral trajectories of recovery and forest

structure metrics derived using field plot measurements combined with high-density (>200 pts/m^2) RPA lidar data in an area impacted by wildfire 16 years prior.

2. Theoretical background

2.1. Spectral trajectories, indices and their components

Spectral trajectories describe the temporal trend of raw band measures or composite indices based on multiple bands. Recent research suggests that incorporating multiple indices and bands in disturbance identification models improves classification because including multiple indices, such as those that capture both landscape greenness and wetness, better capture forest structures (Cohen et al., 2020).

At the broadest scale, visible and near-infrared bands (NIR) capture landscape greenness. Immediately following a disturbance, decreases in live vegetation result in lower NIR and SWIR reflectance, and, generally, higher red reflectance. In the years following disturbance, rapid ingress, usually by forbs and grasses, causes NIR reflectance to increase at rates that are highly correlated with the rate of biomass production (but undifferentiable between short-lived young forbs and tree production) of the landscape (Peterson, 1992). Generally, recovering forests dominated by deciduous components will green faster and earlier but decrease in green and NIR reflectance 15–20 years after the disturbance (Nilson and Peterson, 1994). In the context of our study, in deciduous-dominated areas where forb growth is likely, we would anticipate a rapid increase in greenness focused spectral indices.

The shortwave infrared region of the spectrum and indices which incorporate the shortwave, such as the tasselled cap wetness transformations (Crist and Cicone, 1984), 1984), better capture vegetation structure compared to measures like NDVI, which excludes the shortwave. The inclusion of SWIR describes vegetation stored water (Horler and Ahern, 1986). As forest structure recovers, SWIR reflectance increases. And so, indices like tasseled cap wetness (TCW) trend positive as bare soil and water decrease. As TCW is a strong indicator of changes in forest structure (Cohen and Goward, 2004), we expect more muted temporal increases in regions with high basal area, as basal area is a longer term indicator of a woody recovery. However, tree size and spacing can be highly variable; some areas may have uniformly spaced smaller conifers or irregularly spaced large conifers. Variability in tree spacing and bare ground cover would produce variability in SWIR and associated indices. The variability in SWIR associated indices theoretically describes the interplay between complex forest structure and bare-ground reflectance (Pflugmacher et al., 2012). Additionally, TC indices may improve delineation between broadleaf and coniferous as the higher water stored by broadleaf vegetation will decrease TCW values (Czerwinski et al., 2014;Fig. 1.

3. Study site and data acquisition

3.1. Study location

The Quesnel Timber Supply Area (TSA) is located on the interior Plateau of British Columbia, a mid-elevation (500–1200 m) geographic area with rolling terrain composed of dry interior forests. These dry interior forests are expected to increasingly experience high-severity fires due to both climate change and forest management legacies (Hessburg et al., 2005). The western TSA, where study sites are located, is generally drier than eastern regions, with relatively cool summers and short shoulder seasons (Steen and Coupé, 1997). The western region is split between sub-boreal spruce (SBS) and sub-boreal pine spruce (SBPS) biogeoclimatic zones (Meidinger and Pojar, 1991). Both zones are dominated by hybrid or white spruce (*Picea glauca*), subalpine fir (*Abies lasiocarpa),* lodgepole pine (*Pinus contorta*) in drier areas, and trembling aspen (*Populus tremuloides*) in wetter areas. Historically, these forests have had high-severity burns every 125 years (Biodiversity Guidebook, 1995). However, in the last 20 years, remarkable large-scale disturbances, including wildfires and mountain pine beetle (*Dendroctonus ponderosa*; MPB) infestations, have decimated a large proportion of the Quesnel TSA. Since 2000, an estimated 20 % of the TSA has experienced a stand-replacing disturbance (either from fire or MPB, see Fig. 2; Hermosilla et al., 2016). The 2017 Plateau complex fire, the largest fire in recent BC history, burned approximately 550,000 ha (ha) of the Quesnel TSA (British Columbia Data Catalogue, 2022). Our study sites are located in fires that burned in 2006, before a large-scale MPB outbreak affected many of the other lodgepole pine forests in the region. Two study sites were located in the same fire area, the Watlus Lake fire – which burned ~ 8,500 ha, and a third site in an unnamed fire that burned ~ 10,800 ha.Fig. 2.

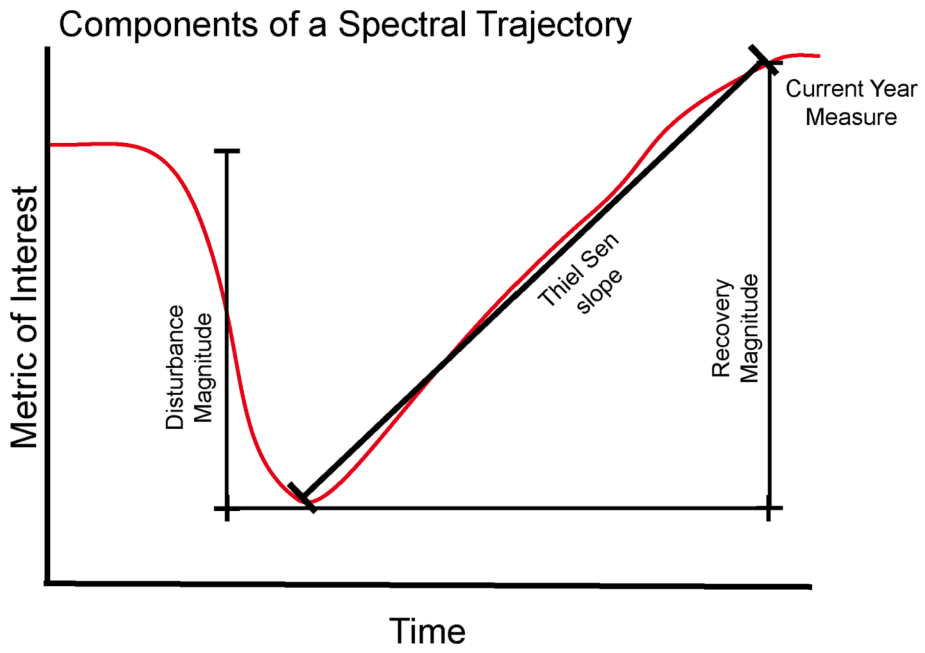

Fig. 1. Example spectral trajectory with four trajectory components labeled with solid black lines. Disturbance magnitude is only included for NBR.

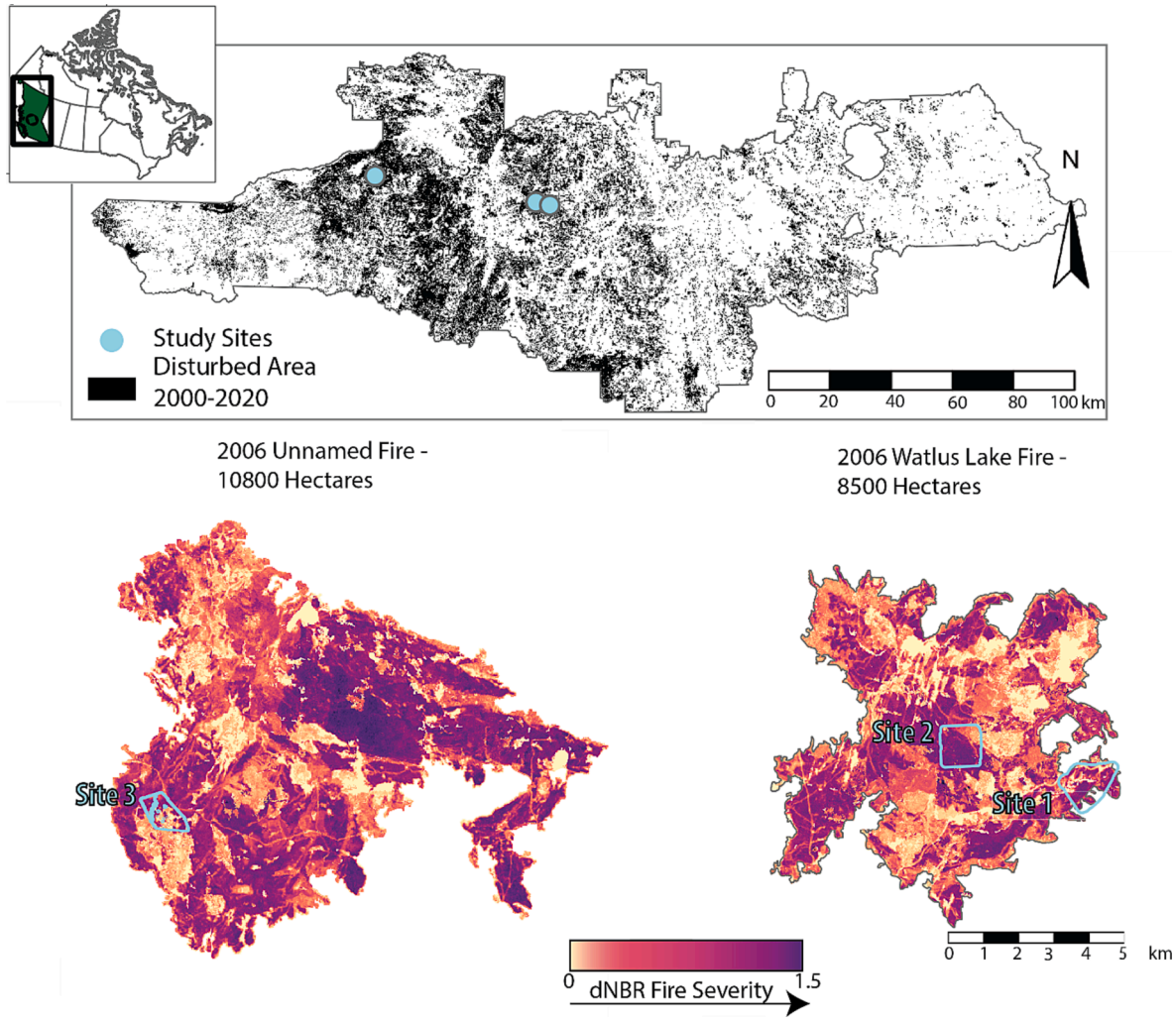

Fig. 2. Top: Location of research sites in Quesnel TSA. Black areas are the disturbed areas (fire, harvest, road, etc) for the past 20 years. Blue dots show the study sites. Below: Outlines of study fires colored by dNBR (delta Normalized Burn Ratio) fire severity (low = yellow, high = purple). Flight areas are outlined in blue. The inset map shows BC study site in reference to Canada. (For interpretation of the references to color in this figure legend, the reader is referred to the web version of this article.)

3.2. Data

To assess whether Landsat post-fire temporal trajectories informed subsequent forest recovery, we combined three distinct data types: (1) time series of spectral data from Landsat composites, (2) ground-based measures of forest structure, which we extrapolated across areas of interest using (3) RPA Lidar (Fig. 3). To simplify analyses, we excluded managed forest areas (i.e., planted or fertilized). To identify areas of high severity fire in 2006 for both field and lidar sampling, we calculated the dNBR and applied existing 'high-severity' thresholds to define dNBR severity classes (BC Ministry of Forests, 2021). The following sections describe acquisition and processing of three data sources: satellite, ground-based measures, and RPA lidar.

3.2.1. Landsat temporal trajectories

Measures of land surface reflectance from space can be obscured by clouds or haze. Composite images combine captures across multiple acquisition dates and offer a way to circumvent no-data areas from clouds or haze on a specific day. We used the Best-Available Pixel (BAP) approach to create cloud-free satellite image composites (White et al., 2014). The BAP compositing approach prioritizes pixels based on a distance to a target day of the year (generally August 1 for Canadian forests, corresponding to peak growing season) and the percent cloud cover and a preference for images from Landsat 8 (White et al., 2014). We created Landsat annual image composites using the BAP compositing approach hosted in Google Earth Engine, prioritizing August 1st with a 30-day date range and a maximum of 70 % cloud cover in a scene (Saverio, 2021). The following spectral indices were generated from BAP composites for each year from 1995 to 2021: NBR (Key and Benson, 2006), NDVI, NDMI (Morresi et al., 2019), and Tasseled Cap transformations of brightness, greenness, wetness, and angle (TCB, TCG, TCW, and TCA, Crist and Cicone, 1984).

We used openly available Landsat-based data products to identify past wildfire locations within our study area (Hermosilla et al., 2016; Hermosilla et al., 2018) open and available for download at: https://opendata.nfis.org/mapserver/nfis-change_eng.html). In these products, wildfires were identified using the Landsat-derived Composite 2 Change (C2C) approach described by Hermosilla et al. (2015). The C2C approach uses a breakpoint analysis of spectra of BAP composites, specifically dNBR, to identify the year of change and post-disturbance spectral trajectories to identify and classify a disturbance. We verified the burn perimeters using a fire polygon data set that catalogues all fires yearly from aerial and satellite imagery (BC Ministry of Forests, 2021).

3.2.2. Field measurements

For our structural data collection, we selected three locations that

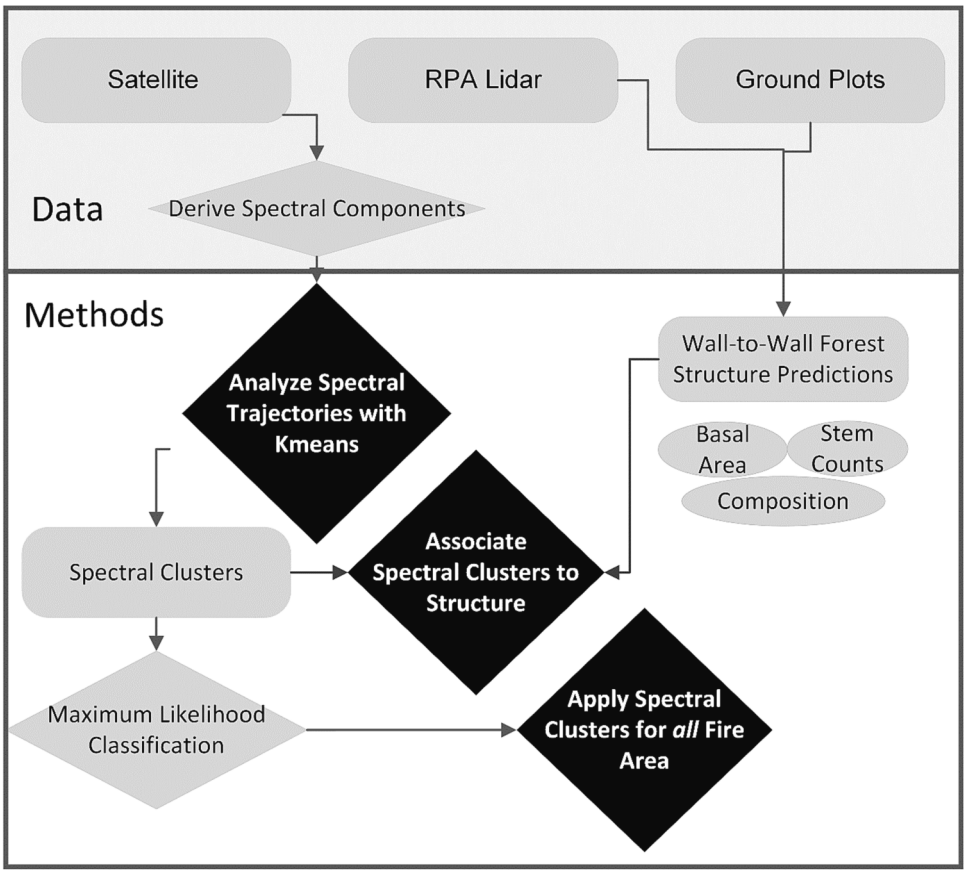

Fig. 3. Conceptual overview of study approach. First section (3. Data) describes data collection including satellite data and estimates of forest structure. Second section (4. Methods) shows model development in three parts: (1) cluster development and assessment, (2) cluster association, and (3) application of clustering to larger fire area.

experienced high-severity fires in 2006. Plot locations were selected randomly from areas that met the high-severity dNBR thresholds. We eliminated random selections that were inaccessible to field crews and not-feasible for RPAS flights. To calibrate lidar-derived forest structural measurements, we measured 26 ground plots in the summer of 2022, coincident with lidar data acquisition. Plots aimed to capture the diversity of forest structure present in the study site as identified via an RPA reconnaissance flight. Precise (5–30 cm) locations of the plot centers were collected by a Trimble Geo7X GNSS unit and corrected using the BC Active Control System base stations. Each fixed area circular plot had a 17 m radius (900 m^2) to correspond to the area of a Landsat pixel. In each plot we recorded the number of stems for all trees greater than 1.3 m tall, the diameter at breast height (DBH) of all stems $\geq$ 4 cm DBH, and the height of the eight tallest trees. Thresholds for height and DBH were based on provincial monitoring standards (BC Ministry of Forests, 2023). We estimated cover by dividing the plot into 8 radial sections and recording the proportion of coniferous, deciduous, and bare earth (which included downed woody debris) that we then averaged at plot level.

3.3. RPA flights and lidar processing

A DJI Zenmuse RPA and L1 lidar system acquired over 430 ha of point cloud data across three sites, which each averaged 155 ha. Lidar system details and flight acquisition parameters are included in Table S1. Lidar data processing used standard workflows, including denoising, ground classification, height normalization, and calculation of point cloud metrics (White et al., 2017b). Progressive ground filtering (Klápště et al., 2020) was used to differentiate between the ground, low-lying vegetation, and coarse-wood. Progressive ground filtering classified returns between 10 and 20 % of returns heights as ground, iterating over increased window sizes (0.25 m, 0.33 m, and 0.5 m) and removing points that would result in dramatic elevation changes (>0.3 m). Obvious and abundant coarse woody debris, which appeared as a linear feature when the ground was poorly classified, informed ground filtering parameterization. Lidar point clouds were georegistered in DJI Terra (version 2.1.6) and exported to Lastools for denoising, classification, and normalization (Isenburg, 2014).

Normalized point clouds from the progressive ground classification were inputs for the final forest metric models. To reduce the variable point density of clouds, we decimated all point clouds to ensure that each 25-m grid had return densities within one standard deviation of the mean number of returns for the entire site area. Lidar point cloud metrics including dispersal (van Ewijk et al., 2011), dispersion, percentiles above varying thresholds (Roussel et al., 2020), and L moments (Karvanen, 2006) were calculated across the field site at a 30 m resolution to match the resolution of Landsat, and for each plot at a 20 cm resolution (for validation).

4. Methods

To assess structural forest recovery over large scales, we created wall-to-wall estimates of forest structure for selected study sites using lidar data. These estimates were used to investigate the ability of temporal trajectories of satellite spectra to discern distinct expressions of forest structure. Our investigation is divided into three steps: cluster analysis, association with structure, and application of clustering to a larger fire area (Fig. 3).First, we derived post-fire temporal trends of Landsat spectral measures for the seven selected indices (Table 1) from 2005 to 2021. Temporal trends (trajectories) were delineated into

Table 1
Definition of selected indices and their expected relationships between spectral trajectories of indices and robust recovery of forest structural metrics. B – blue, G-green, R – red, NIR – near infrared, SWIR1 – short wave infrared 1, SWIR 2 – short wave infrared 2. Saturation is the point where the sensitivity of the metric decreases. For NDVI, this is when red absorption is high. In NBR and NDMI this is when SWIR and NIR are equal.

Index	Description	Equation	Reference for Spectral Response	Reference Forest Type
NBR	Normalized Burn Ratio	$\frac{NIR - SWIR2}{NIR + SWIR2}$	(Hermosilla et al., 2015; Nguyen et al., 2020)	Boreal, Dry Deciduous
NDVI	Normalized Difference Vegetation Index	$\frac{NIR - R}{NIR + R}$	(Vanderhoof and Hawbaker, 2018)	Dry coniferous
NDMI	Normalized Difference Moisture Index	$\frac{NIR - SWIR1}{NIR + SWIR1}$	(Senf and Seidl, 2022)	Coniferous and mixed broad leaved
TCA	Tasseled Cap Angle	$\arctan\left(\frac{TCG}{TCB}\right)$	(Pflugmacher et al., 2012)	Mixed-Conifer
TCG	Tasseled Cap Greenness	$-0.1603B - 0.2819G - 0.4934R + 0.7940NIR - 0.0002SWIR1 - 0.1446SWIR2$	(Coefficients of: Crist and Cicone, 1984; implemented in: Pflugmacher et al., 2012)	Mixed-Conifer
TCB	Tasseled Cap Brightness	$0.2043B + 0.4158G + 0.5524R + 0.5741NIR + 0.3124SWIR1 + 0.2303SWIR2$	(Coefficients of: Crist and Cicone, 1984; implemented in: Pflugmacher et al., 2012)	Mixed-Conifer
TCW	Tasseled Cap Wetness	$0.0315B + 0.2021G + 0.3102R + 0.1594NIR - 0.6806SWIR1 - 0.6109SWIR2$	(coeffiences of: Crist and Cicone, 1984; implemented in: Nguyen et al., 2020)	Dry Deciduous

segments, henceforth referred to as trajectory components. Components were used as inputs into a kmeans data-clustering algorithm that identified unique clusters of spectral trends. Second, we assessed the association between each trajectory cluster and three wall-to-wall structural metrics derived from the RPA and field data: (1) BA, (2) stem counts, and (3) coniferous to deciduous ratio. Third, we applied the clustering algorithm across a burned landscape where there are no historical structural measures.

4.1. Wall-to-wall forest structure predictions

From RPA lidar data, we estimated three silviculture measures of forest structure (BA, stem counts, and the coniferous to deciduous ratio) using generalized linear models (GLMs). GLMs correlated field measures with lidar metrics such as L-moments, dispersion, cover, and other standard height metrics as listed by Falkowski et al. (2009). Our wall-to-wall approach was based on best-practices outlined by White et al. (2017). BA models used a two-step segmented model process which first modeled the probability of measurable BA from a logit link function. BA models were augmented with plot measures in undisturbed forests to ensure that the model was accurate in regions with a higher BA. For stem count models, we used zero-inflated negative binomial regressions that estimated the number of stems > 1.3 m for each Landsat pixel. This included a conditional model that first calculated the likelihood that there were stems in the plot and then a model for the number of stems in each plot. Predicted stem counts represent the number of stems in the size of each Landsat pixel (900 m^2; hereafter stems/pixel). Finally, we used a beta regression to model the coniferous: deciduous ratio.

For all models, lidar metrics with strong inter-correlations (Spearman correlation > 0.7) were not used. Final reported model coefficients and accuracy were output from a k-folds algorithm with 100 iterations. Final model predictions across the study area were built from model coefficients and represented spatially-explicit estimates of BA, stem counts, and percent conifer for the entire area of RPAS data at each site.

4.2. Unique satellite spectral trajectories from cluster analysis

4.2.1. Clustering of spectral trajectories

The clustering algorithm incorporated three spectral trajectory components computed for the seven Landsat spectral indices (NDVI, NBR, NDMI, and the tasseled cap transformations: TCB, TCG, TCW, and TCA) for each pixel within the study area. Our selection of spectral indices was based on a review of the literature for the most pragmatic indices for both disturbance classification and subsequent forest monitoring (Hermosilla et al., 2015; Nguyen et al., 2020; Pflugmacher et al., 2012; Senf and Seidl, 2022; Vanderhoof and Hawbaker, 2018; listed in Table 1). Trajectory components were based on those of Nguyen et al.. (2018) and White et al., (2017a) and included: (1) the magnitude of change between the year of disturbance and 2021 (recovery magnitude), (2) the Theil-Sen slope of the post-disturbance spectral trajectory, and (3) the spectral value for the index in 2021 (see Fig. 1; Nguyen et al., 2018). Given the heterogeneous nature of fire severity, several patch-level metrics, including burn severity (dNBR) and a spatial average of burn severity, were included to better represent known ecological recovery patterns within a forest stand. In total, there were 23 separate trajectory components. Given the high dimensionality of the data, we partitioned clusters using the Manhattan distance (Aggarwal et al., 2001). We selected an optimal number of clusters using the gap statistics which suggested ten initial seeds. The gap statistics measures the increase in explanatory power between n and n + 1 clusters (Hennig, 2020). Final cluster centers were outputs of a kmeans algorithm with a maximum iteration of 200. Cluster similarities were tested using cluster bootstrapping with 100 iterations of the Jaccard index (Hennig, 2020). Clusters that shared NBR recovery slopes were merged, which eliminated similar clusters.

Spectral characteristics of each cluster were investigated using a Principal Component Analysis (PCA), including the coefficients associated with the PCA transformation or the PCA loadings. Following the PCA analysis, we investigated the averages of trajectory components for each cluster. Spectral indices were related to the relative difference from a baseline period – defined for a stable forest period 1996 – 2005. As we were most interested in associating structural characteristics with each cluster, we constrained initial clustering to areas within RPAS lidar acquisition flights. To then extend the kmeans clusters to other areas within the fire perimeters, we applied a maximum likelihood classification using the same inputs as kmeans, where classes were defined by initial clustering (Richards and Jia, 2006). We used the original kmeans cluster area to develop 80 % training (N = 3615) and 20 % testing (N = 1445) data. The final maximum likelihood accuracy was assessed by comparing the accuracy of the classifier with the test data. We also assessed the contiguity of spectral clusters on the landscape using each cluster's total and patch area size and proportions (where a patch would be a pixel with eight identical neighbors). The Landscape metrics' R package was used to estimate cluster continuity on the landscape (Hesselbarth et al., 2019), with differences in forest structure assessed among spectral clusters using the FSA R package (Ogle et al., 2022).

4.2.2. Relating spectral trajectory cluster to forest structure

We characterized cluster trajectories based on BA, stem counts (stems/pixel), and the ratio of coniferous to deciduous (coniferous: deciduous). Tests for differences in forest structure among clusters used a Kruskal-Wallis nonparametric test and a two-sided post hoc Dunn test using the Sidak correction to control for error among multiple

comparisons (Dinno, 2017). All modelling was completed using base R stats (R Core Team, 2019), 'betareg' (Cribari-Neto & Zeileis, 2010; Grün et al., 2012), and 'glmmTMB' packages (Brooks et al., 2017).

5. Results

5.1. Wall-to-wall forest structure predictions

Linear models successfully described the relationships between lidar estimates and field measures (Table S2). Field measured plots had an average BA of 6.8 ± 8.65 m^2/ha, 0.08 ± 0.21 % coniferous, and average stem count of 321 ± 294 (stems/pixel). For linear estimates of these models, BA had the strongest agreement with field measures (R^2 = 0.95), but was variable due to the high proportion of plots with low BA (RMSE = 6.285). This was followed by predicting whether an area had measurable trees (area under the curve (AUC = 0.79). The overall fit of the stem count model was moderate (R^2 = 0.52, RMSE = 121). The coniferous:deciduous ratio had the lowest correlation to field data with a pseudo-R^2 of 0.41 (RMSE = 0.11).

Similarly, sites displayed variability in wall-to-wall estimates of structural recovery (Figure S2). Across all sites, 66 % of pixels had a measurable basal area (>0 m^2/ha; Table 2). In general, estimates of the average basal area were variable within and across sites (average = 0.77 ± 0.81 m^2/ha). Stem count estimates were also variable (596 ± 500 stems/pixel). Overall, the sites were primarily coniferous, with all the sites having more than 50 % coniferous stems (Table 2). Fig. 4 shows the spatial variation in the forest structure of site 1 (located in the Watlus Lake fire), which exhibited similar structural variability compared to the other study sites (see Figure S3 and S4 for site 2 and site 3).

5.2. Clusters of unique spectral recovery trajectories

The clustering algorithm identified six unique spectral clusters that captured 81.6 % of the variation in the input data for the study sites. Fig. 5 shows a biplot of the first two principal components of a PCA on clustering analysis data. The first and second PCs collectively represented 68 % of the total variability in the data set. When scaled based on the proportion of variance, important metrics to describe dataset variable (principal component loadings) included the Thiel Sen slope of NBR, TCA, and NDMI, and the regrowth of TCA and NBR (for a complete list of eigenvectors see Table S3). In the PCA plot, clusters 2 and 3 have the highest spectral overlap, and clusters 1 and 6 are the most distinct (Fig. 5).

Fig. 6 shows the trajectories of spectral indices following the fire normalized to a pre-fire baseline (1996–2005). Most indices show similar trends with trajectories decreasing after disturbance, rapidly increasing, and plateauing to steady recovery at or above baseline values. Changes were most rapid for NDVI and TCB, most TCB values surpassed baseline less than a year after the disturbance. (Table S4). Conversely, NBR and TCA trajectories increased at slower rates. In cluster 1, both NBR and TCA took > 10 years to surpass baseline values (Fig. 6). Notably, the majority of NDMI and TCW pixels did not recover to pre-baseline values in most clusters (Table S4).

Clusters generally exhibited similar temporal patterns of spectral recovery, but clusters were variable in their degree and magnitude of recovery. Cluster 2 and 3 had the greatest variability for within-year measures (shown by the line width of Fig. 6) and often overlapped the range of values in other clusters. In general, clusters 5 and 6 had the highest values for most spectral indices (Fig. 6). Cluster 1 had the largest decrease after the disturbance event and took the longest to surpass baseline values. Additionally, less than 10 % of pixels in cluster 3 surpassed values of baseline for TCA and NBR in 2021–15 years after the disturbance. More than 50 % and at least 10 % of pixels in other clusters (1,2,4,5,6) surpassed baseline values for NBR and TCA respectively (Table S4).

Average trajectory components for measurement year (2021), regrowth magnitude, and Thiel Sen slope (Fig. 7) differed by spectral cluster. For the current year measure, cluster 6 had the highest index measures and cluster 3 had the lowest, except for TCB (Fig. 7 and Table S4). Regrowth magnitudes were highest for cluster 6, except for TCB, where cluster 3 is the highest (Fig. 7). Cluster 6 generally had the lowest slope of recovery for all indices. Similar to regrowth magnitudes, the average Thiel Sen slopes were highest for cluster 6, except the average TCB slope, which was highest for cluster 2. Clusters 2 and 3 had similar average magnitudes of recovery for both TCG and TCB (Table S4). Clusters 2 and 3 also had lower recovery slopes than cluster 1, except for TCB where cluster 2 was higher. Slopes of recovery for NBR, NDMI, NDVI, and TCA were all significantly different ($p < 0.1$, Table S4).

5.3. Relating spectral clusters and measures of forest structure

Spectral clusters represented significantly different measures of forest structure (Fig. 8 and Table 4). BA estimates were highest for cluster 1 (0.85 +/- 0.72 m^2/ha), and lowest for cluster 6 (0.22 m^2/ha). All clusters had unique counts of coniferous stems per Landsat pixel. Cluster 3 had the highest stem densities (750 ± 402), followed by Cluster 1 (623 ± 428), and Cluster 6 had the lowest (222 ± 266; Table 3). Areas with high stem counts and/or BA were spatially distinct from regions with a high deciduous composition (i.e., clusters 1 and 3 are distinct from cluster 6). For composition estimates, cluster 1 had the highest proportion of coniferous stems (96 %), followed by cluster 2 (89 %). Cluster 6 had the lowest coniferous to deciduous ratio (56 %).

5.4. Spectral clusters applied to fire landscape

Fig. 9 shows a maximum likelihood classification of the spectral clustering in relation to the 2006 Watlus Lake fire perimeter which expands from the original clusters constrained to areas with forest structure measures. The overall classification accuracy was 0.83 % (Table S5). Cluster 1 was the most commonly occurring cluster, covering 33 % of the land area (Table 3). Cluster 3, the least common cluster, accounted for 8.2 % of the land area and had the fourth- largest average patch size (5.33 ha), where a patch denotes an area of at least 8x8 pixels. Cluster 4 had the smallest average patch size (4.52 ha). In the classification, cluster 1 was the most accurately classified (user accuracy = 0.91; producer accuracy = 0.88, Table S5), and cluster 6, which represented the second smallest proportion of the landscape, was the least accurately classified (user accuracy = 0.7, producer accuracy = 0.68). Clusters 5 and 6, which were generally spatially grouped (Fig. 9), were frequently misclassified as one another (Table S5). In general, areas of high BA (clusters 1,2,3, and 5) were grouped and proximal to areas with

Table 2
Average structural metrics by pixel for each study site and averages for all study sites. +/- is the standard deviation among the site.

Site #	Basal Area (m^2/ha)	+/-	Coniferous: Deciduous	+/-	Stem Counts (stems/900 m^2)	+/-	Proportion w/ Basal Area
1	0.56	0.72	0.87	0.19	556	463	0.63
2	1.00	0.86	0.98	0.08	650	523	0.81
3	0.21	0.48	0.72	0.32	230	243	0.51
All Sites	0.62	0.78	0.87	0.23	509	472	0.66

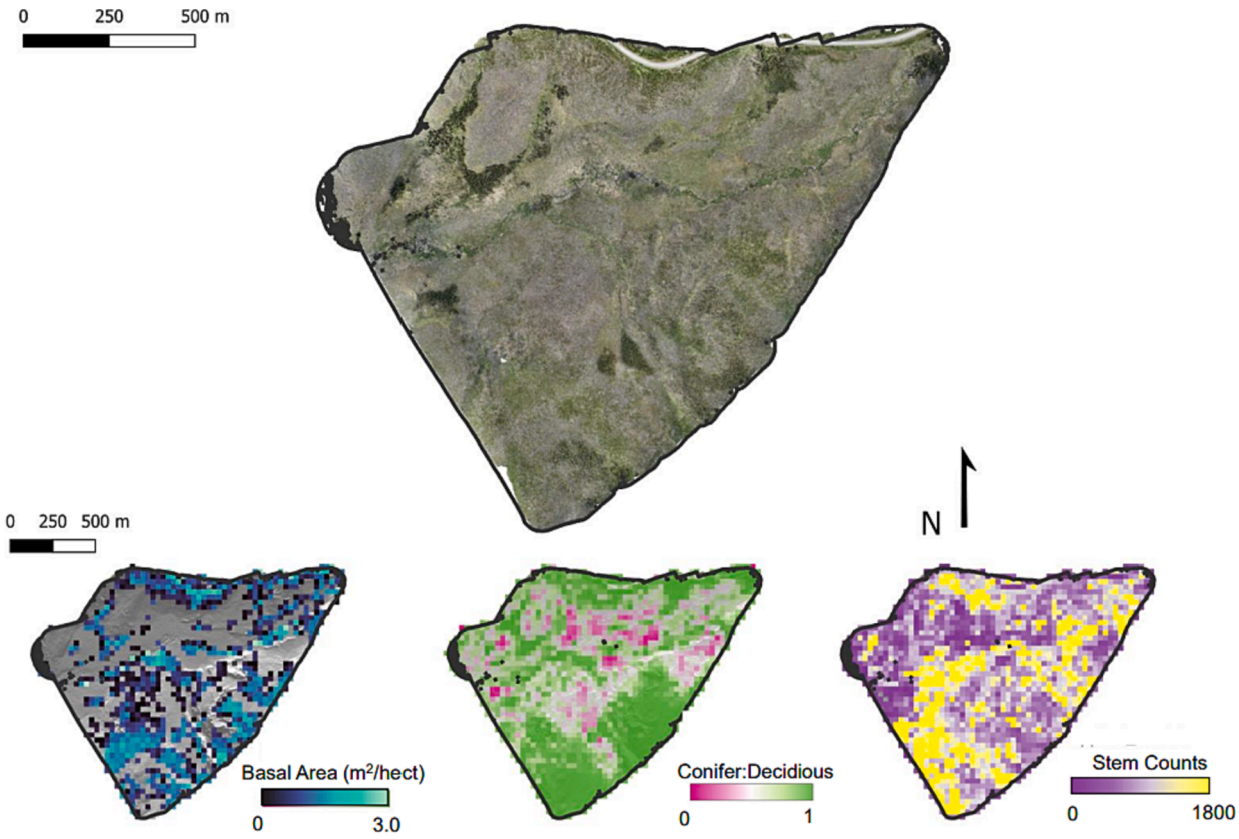

Fig. 4. Example output of lidar structural model for Site 1. Rasterized models are shown below an orthographic photo and are colored according to the estimate of forest structure. Examples for site 2 and site 3 are located in the supplement.

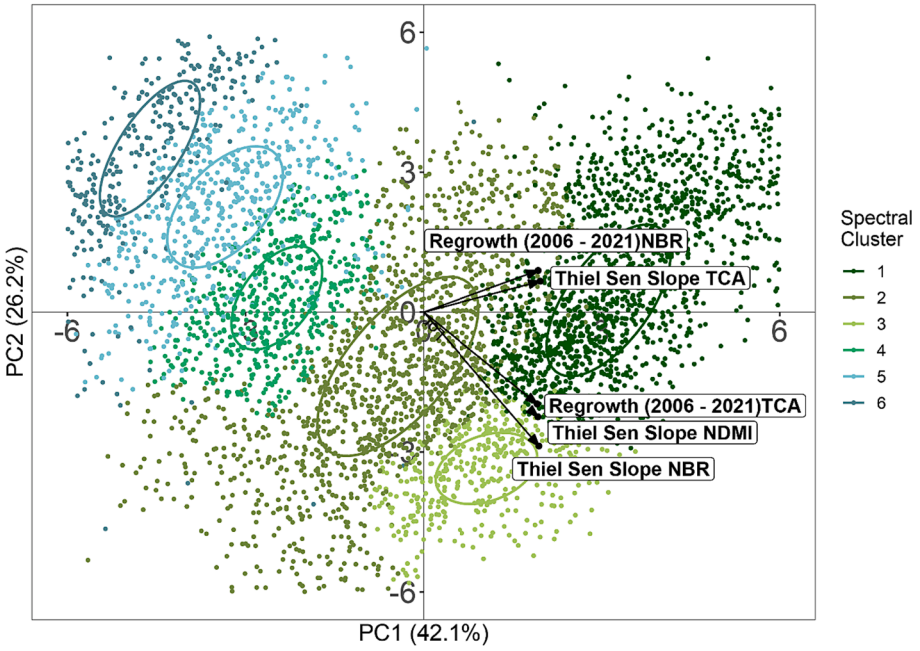

Fig. 5. PCA of pixels based on spectral indices. Points are colored by spectral clusters. Ellipses show where 50% of the data plots. Loadings are the scaled proportion of variance in PC1 and PC2. Ellipses represent the locations where 50 % of pixels from each cluster plot.

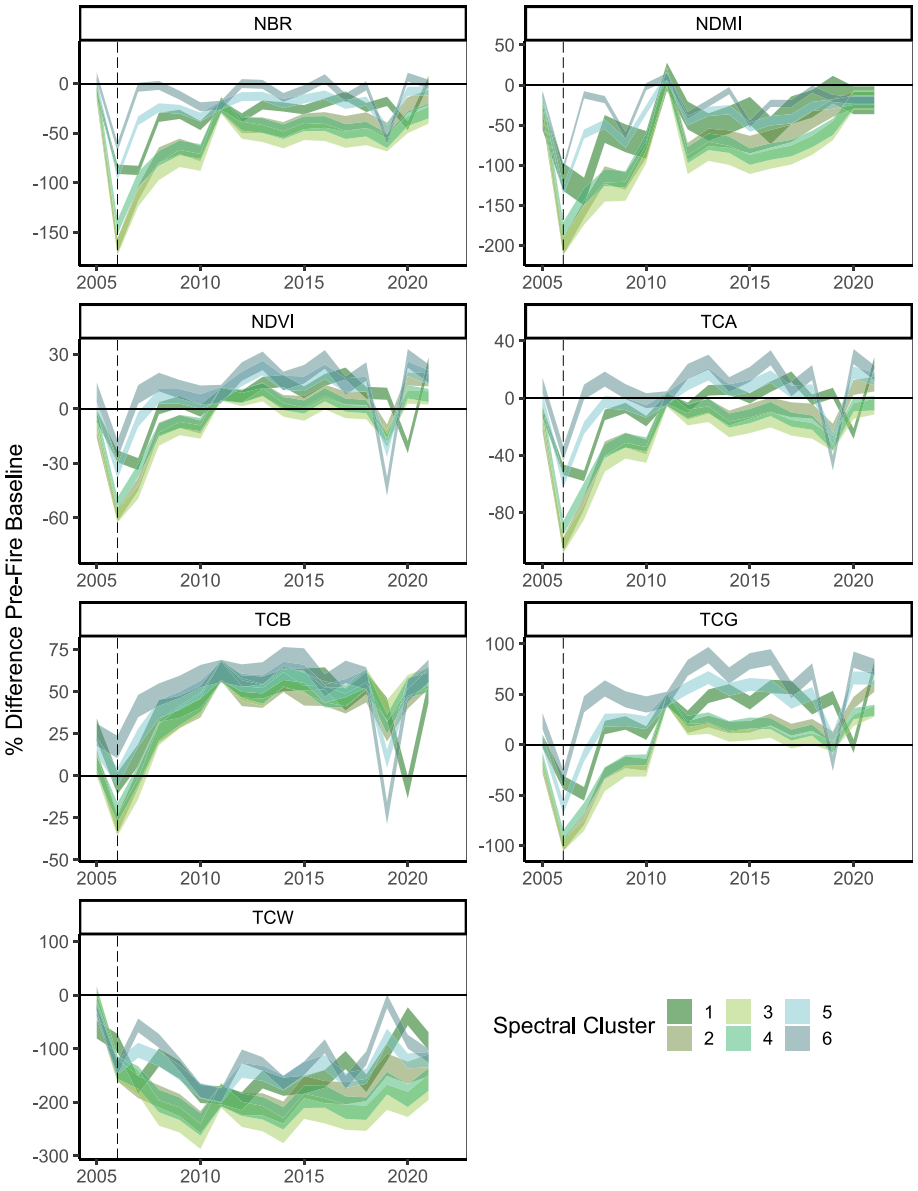

Fig. 6. Spectral trajectories input to create 6 (shown in color) spectral clusters. "Pre-fire baseline" refers to the 10-year period preceding the fire (1995–2005). Values are the difference (%) from the pre-fire baseline before the disturbance, where 0 (black line) is no difference from baseline measures. Yearly values are two-year moving averages, with the line width equal to the standard deviation by spectral cluster and band. The vertical dashed line is the year of the fire (2006).

a high number of conifer stems - like cluster 3 (cluster 1 and is adjacent to cluster 3 Fig. 9).

6. Discussion

This study used temporal trajectories of various Landsat spectral indices to identify distinct types of post-fire spectral recovery that describe variants of post-disturbance forest structure. Such research is critical because the increasing frequency and severity of wildfires make ground assessments a difficult singular monitoring strategy (Huang et al., 2019), and satellite monitoring approaches struggle to capture distinct and important silviculture measures (Chu and Guo, 2014). The variable forest spectral types we observed corresponded with variable predictions of forest structure derived from integrated field plot measurements and high-density RPA lidar data. Specifically, some clusters (e.g., cluster 1) demonstrated a higher proportion of coniferous recovery than spatially adjacent clusters (namely cluster 3). Cluster 3 had high coniferous stem densities, but also a higher proportion of deciduous species. Spectrally distinct locations where coniferous recovery is lower, like cluster 3, may represent areas transitioning from coniferous to mixed forest types (Epting and Verbyla, 2005; Hayes and Buma, 2021). Cluster 3 also returned to baseline values of NBR in an average of 5 years, whereas cluster 1 took more than 13 years. The unique spectral trajectories we identified using kmeans clustering showcase our capacity to monitor structural differences, particularly those relevant to forest management, using spectral measures. With large-scale and intense fires in northwestern North America, recovery monitoring must capture spectral signatures that signal a transition from pre-disturbance stands (e.g., those dominated by lodgepole pine) to those with a higher proportion of deciduous trees (Hayes and Buma, 2021; Kiel and Turner, 2022; White et al., 2023).

Relevant benchmarks for strong coniferous recovery are defined by historical work in similar xeric subalpine fire-prone forests. A recent BC study surveyed carbon sequestration and stem densities 10 to 60 years post-fire and found young regenerating forests had highly variable stem densities, anywhere from 100 to 10,000 stems/ha (Clason et al., 2022),

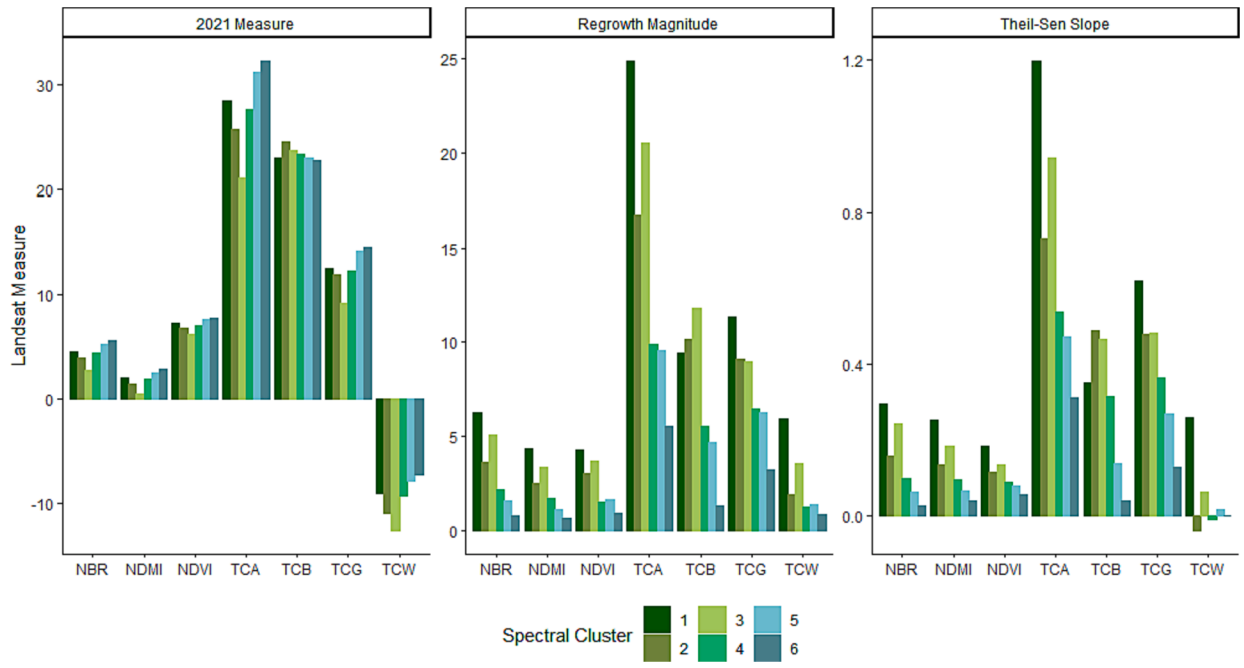

Fig. 7. Differences between average trajectory components for each cluster among seven unique bands. Color shows the associated spectral clusters. 2021 Measure is the summer 2021 Landsat measure, regrowth magnitude is the overall change from 2006 to 2021, and the Thiel Sen slope is the estimate regression line between 2006 and 2021. Note: to allow metrics to plot on similar scales NBR, NDMI, and NDVI are multiplied by 1000.

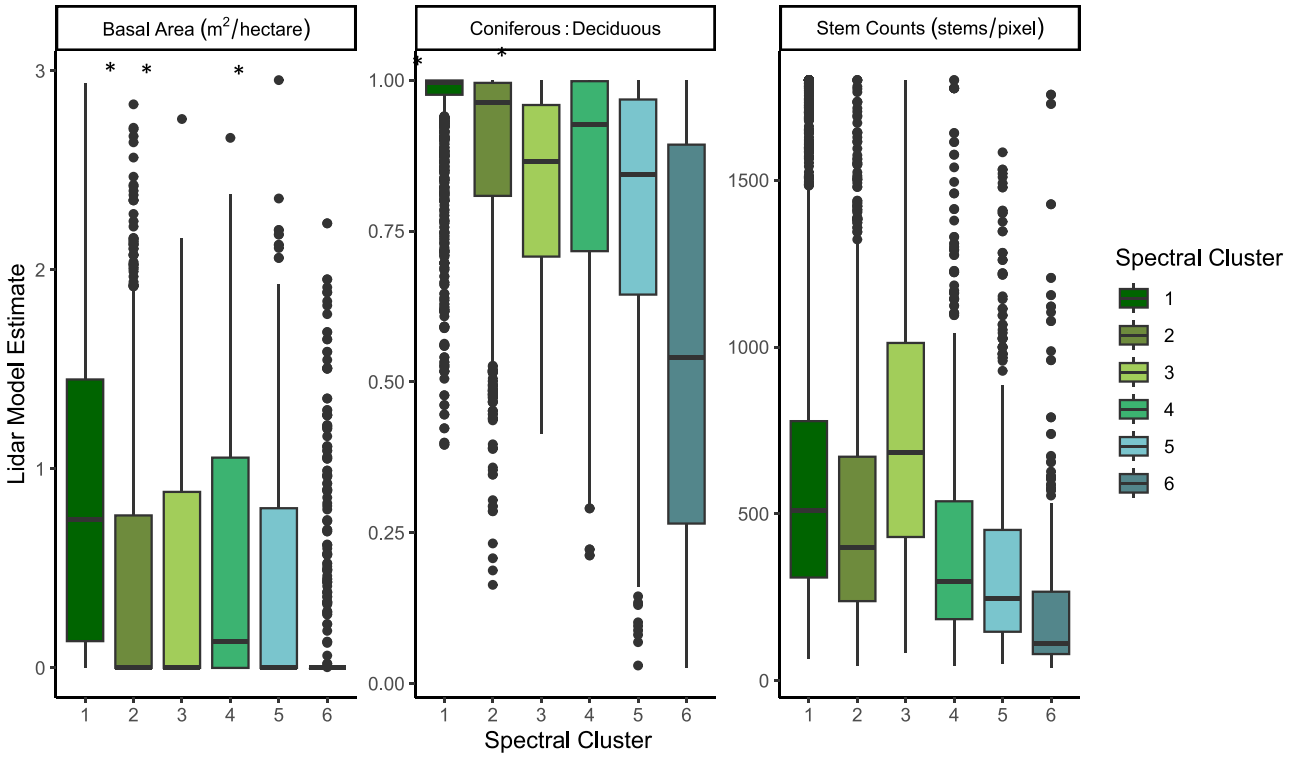

Fig. 8. Distribution of structural metrics: Basal Area (m^2/ha), stem count (stems/pixel), and the coniferous:deciduous ratio. Boxes note the interquartile region and black lines are the median values. Columns that share symbols are statistically similar (Dunn test $p < 0.05$).

or 90 to 900 stems per Landsat pixel. Our results were similarly variable; many of the clusters had high stem counts (average stem counts are all greater than 200 stems per pixel), but the stem count estimates were also highly variable. A *meta*-analysis of post-fire recovery in dry coniferous forests of Colorado found BA was generally greater than 0.2 m^2/ha twenty years after a fire event (Donnegan and Rebertus, 1999). In our work, all clusters had an average BA higher than 0.2 m^2/ha, but, similar to stem counts, responses were variable. It should be acknowledged that many studies of forest recovery opt to include trees below breast-height in BA calculation (e.g. Clason et al., 2022). However, the BA variability we observed has also been found in other models of early forest recovery. For example, a Canada-wide study that included post-disturbance

Table 3
Landscape and structural metrics for each spectral cluster. Values are the average for each cluster (+/- standard deviation). Study area refers to area covered by lidar flights and Fire area is the entire 2006 Watlus lake fire perimeter.

Cluster	Coverage (%)	Study Area Mean Area (ha)	+/-	Fire Mean Area (ha)	+/-	Basal Area (m^2/ha)	+/-	Stem Counts (stems/ pixel)	+/-	Coniferous: Deciduous (%)	+/-
1	32.7	7.31	1.52	6.67	1.05	0.85	0.71	623	428	96	9
2	27.8	5.39	0.89	6.80	0.87	0.42	0.61	503	352	89	15
3	8.2	5.91	1.00	5.33	0.79	0.42	0.57	750	402	82	16
4	11.2	3.48	0.28	4.52	0.47	0.52	0.63	421	343	84	20
5	10.3	4.11	0.27	5.13	0.63	0.42	0.60	356	303	78	22
6	8.4	5.72	0.65	6.27	0.90	0.22	0.47	222	266	56	32

Table 4
Outputs of Chi-Squared test and Dunn test for each structural metric. Only pairs that are statistically similar are listed (based on a P-value < 0.05).

Variable	Chi Squared Test	Like Pairs (Dunn-test)	Adjusted P-Val
Basal Area	$X^2(5, N = 6492) = 781.23, p = 0$	2–5, 2–3	1
Stem Counts	$X^2(5, N = 6492) = 1194.69, p = 0$	All Unique	
Composition	$X^2(5, N = 6492) = 1515.42, p = 0$	2–4	0.59

basal area modeled a negative BA up to 10 years post-disturbance, but most forests were greater than 3.3 m^2/ha 20 years after a disturbance. The dramatic change in BA in-between estimates at 10 and 20 years by Bartels et al. (2016) and the variability in BA within and among our spectral clusters suggests 10–20 years after a fire event, the forests undergoes a period of rapid, but spatially variable BA growth. Spatial variability could result from site-level differences such as soil moisture. The study by Clason et al. (2022) found BA was highly variable based on moisture dynamics. We did not consider the variability in BA associated with soil moisture dynamics, and support that soil moisture is an important area of future research to better understand recovery dynamics (Talucci et al., 2019).

6.1. *Clusters derived from spectral trajectories capture unique post-disturbance recovery*

The six distinct spectral recovery clusters derived from the trajectories of Landsat time series indices represent a range of young post-fire forest recovery responses. The most frequently occurring cluster (cluster 1) covered 33 % of the area within the fire perimeters, had the greatest BA and the greatest coniferous proportion. Regions with strong coniferous recovery, such as cluster 1, were spectrally defined by a relatively slow but consistent spectral recovery from 2006 to 2021. Such recovery patterns are consistent with other landscape studies, which show dense coniferous forests have longer recovery times and a greater change magnitude or slope of recovery than mixed and broadleaf forests (Epting and Verbyla, 2005; White et al., 2023, 2022). We assessed the degree of recovery as a measure of return to a 10-year baseline, longer than some other studies looking at post-fire recovery (Gómez et al., 2014; White et al., 2017a). Disturbances in the baseline period would influence recovery dynamics, because landscapes recover differently from multiple disturbances (Kiel and Turner, 2022; Nguyen et al., 2018). However, prior to the fires at the research sites, the landscape did not undergo any major disturbances including harvest or wildfire (Zhu et al., 2020). While we believe that a 10-year baseline was acceptable for our research purposes, the overall influence of baseline period on spectral recovery is

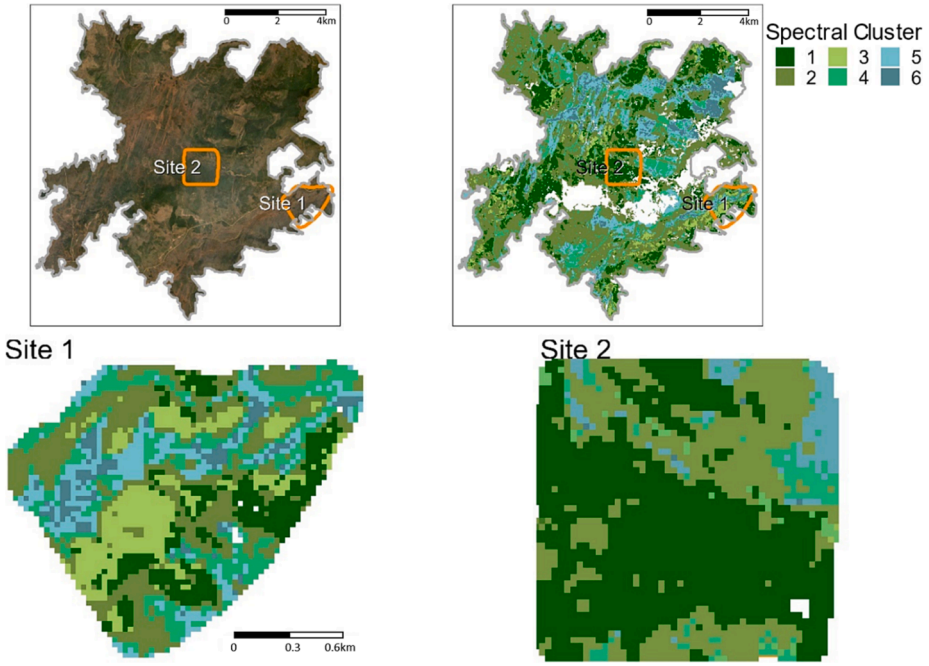

Fig. 9. Spectral classification 2006 Watlus Lake fire recovery. Sites covered by lidar are outlined in orange. White areas did not have enough spectral coverage for classification. (For interpretation of the references to color in this figure legend, the reader is referred to the web version of this article.)

important, as variability of ecosystems' spectral values are highly site-specific (Pasquarella et al., 2016).

The spectral responses for areas with low coniferous ingress behaved similarly across all indices. Clusters where deciduous growth was more pronounced (clusters 3, 5 and 6) had rapid spectral recovery of NDVI, NBR, NDMI, and TCG that then plateaued at or slightly above historic baseline values. Cluster 6, which had the lowest proportion of BA, stem counts, and coniferous ingress, exemplified this swift spectral recovery. A review of RPA orthophotos collected coincident with lidar data indicated that cluster 6 was located in wetlands; this was verified by the negative regrowth in TCW related to water reflectance (Crist and Cicone, 1984). A study that assessed the utility of various indices to differentiate between deciduous, harvested, and closed canopy stands found that TCW was best at identifying deciduous forest types (e.g., *Populus spp*), where leaf water concentration is more dominant in spectral responses (Czerwinski et al., 2014). Rapid recovery of cluster 6 was likely associated with deciduous species, including willows or trembling aspen (*Salix spp* or *Populus tremuloides*), either not consumed in the fire, or that regrew or resprouted rapidly (Bartels et al., 2016; Dymond et al., 2002). Clusters 4 and 5 exhibited similar rapid spectral recoveries and eventual plateaus, but were generally less pronounced than the spectral recovery patterns of cluster 6.

The low recovery slopes and 2021 spectral index values for cluster 3–6 compared to cluster 1–2 suggest regions with high deciduous growth coincide with accelerated spectral recovery (for NBR, TCA, TCG these clusters surpassed baseline early on post-disturbance compared to clusters 1–3). The rapid spectral recovery associated with strong deciduous growth is consistent with past research, including a multi-year study of boreal forests where fast spectral recovery also corresponded to deciduous growth (White et al., 2023). Further, the rapid recovery of TCG and TCA corresponds with a Canada-wide study reviewing different spectral indices for post-disturbance monitoring which found that measures like TCG, which rapidly recovered and then stagnated, were advantageous for monitoring deciduous ingrowth (Pickell et al., 2016). However, the same study found that measures such as NBR were slower to stagnate and, thereby, better for monitoring structural non-deciduous recovery (Pickell et al., 2016). We found that NBR and TCG, when analyzed in combination, were both informative of rapid deciduous recovery, a rapid recovery that stalls several years after disturbance.

Select indices were particularly useful for differentiating between distinct landscape trajectories and structural recovery. TC indices (namely TCW), use visible, NIR, and SWIR, transformed into a singular value for landscape brightness, wetness, and greenness. These indices helped differentiate among areas of similar greenness, where one is coniferous and one is deciduous (Horler and Ahern, 1986). For example, all clusters had lower TCW slope estimates except cluster 1, which was 25 % greater than other metrics (Table S4). The large change of TCW slope for cluster 1, which was dominated by conifers, was likely the result of the strong evaporative control by conifers which would increase TCW (Moreno-Fernández et al., 2021). Cluster 2 had similar proportions of coniferous growth compared to cluster 1 but had a lower basal area and stem counts. The minor change in TCW of cluster 2 was likely due to a decrease in conifer density. Another index useful to differentiate between cluster 1 and 2 was TCB. TCB was the only index where the magnitude and slope of recovery of clusters 2 and 3 were higher than that of cluster 1. TCB values are likely higher because clusters 2 and 3 had lower basal area estimates than cluster 1. Higher TCB values are expected for clusters 2 and 3 because TCB is related to soil reflectance, which would decrease at higher basal areas (Horler and Ahern, 1986). This is confirmed by another study that estimated basal area from a single year of Landsat data in dry forests of eastern Oregon, where authors found TCB had a strong negative correlation with basal area (Pflugmacher et al., 2012). Similarly, in the current study, areas of higher TCB growth corresponded to areas with lower basal areas (Fig. 8).

6.2. Relative importance of spectral indices are a consequence of multispectral approach

Our results using trajectories from multiple spectral indices showed promise delineating variable forest recovery using components of spectral trajectories. Other studies, like Nguyen et al. (2018), use a similar combination of trajectory components of NBR to investigate recovery trajectories from diverse disturbance types in Victoria, Australia. Nguyen et al. (2018) also incorporated the Recovery Indicator (RI), a ratio of the change in NBR at 5 years post disturbance to the disturbance severity (Kennedy et al. 2012), instead of the magnitude of regrowth as we used. We excluded the RI in our analysis because preliminary investigation suggested that including the recovery indicator in clustering decreased the explanatory power of the kmeans algorithm on our spectral trajectory data. As the Recovery Indicator is normalized to disturbance severity, it is designed to compensate for areas with lower pre-fire NBR or for lower magnitude changes and is thereby useful for highlighting landscape-level differences in post-disturbance recovery across large geographic areas at 5 years post disturbance (Kennedy et al. 2012). As our analysis focused on two fire events within similar biogeoclimatic conditions and forest types, such broad landscape-level differences were not captured in our dataset. Future research is needed to investigate whether the importance of different satellite indices, as a descriptor of forest recovery variability, is altered by changes in forest types and biogeoclimatic conditions.

The importance of tasseled cap indices for differentiating among structurally divergent landcover was consistent with previous work (Dymond et al., 2002). However, our results exhibited distinct patterns associated with our multi-index approach (Cohen et al., 2020; Viana-Soto et al., 2020). The ability of TCA to differentiate between structures in young forests could result from the metric representing a ratio of soil reflectance (TCB) to vegetation growth (TCG). However, other studies have found TCA less important than other indices. Specifically, Viana-Soto et al. (2020) used TCA and TCW to monitor decreases in forest health after fire events. They found that TCW detected the forest structure better and that TCA measures often became saturated as the forests matured. Similarly, Cohen et al. (2020) demonstrated that TCW was the best at disturbance and recovery identification even when other indices, such as NBR and NMDI, were included. Another study modeled aboveground biomass and found TCA was particularly advantages for modeling forest density in low-biomass highly dynamic forests (Gómez et al., 2014). As our field locations were located in a high-severity fire area and had overall low basal area, the local conditions could explain the overall importance of TCA as the most vital cluster determinant for PC1 and PC2 compared to the inverse results of Cohen et al (2020) and Viana-Soto et al. (2020). Further, Fornacca et al. (2018) studied burn scar identification more than five years after a fire. They found that NDMI and NBR were best able to measure variable conifer responses (Fornacca et al., 2018). The importance of NDMI in our study alongside the work of Fornacca et al. (2018) supports that incorporating NDMI into the multivariate assessment of structural recovery may better elucidate variable conifer recovery than TCW and TCA alone. Campos-Taberner et al. (2023) show that land use classification improved when using textural measures of NDVI for land use classification, suggesting one method to circumvent the spatial complexity of the spectral response is to integrate textural information of surrounding pixels. In general, spectral observations are influenced by the vegetation composition of the landscape and results should be applied with caution in areas where the severity of the fire is lower.

6.3. Utility of RPA lidar for post-disturbance structure modeling

Our work is an important contribution to research using lidar data to model structural forest recovery in young forests. Short and diverse forests are notoriously difficult to model with lidar data (Ørka et al., 2016). In particular, the accuracy of modeling important attributes like

tree height and stem counts decreases when trees are shorter, due to uncertainty defining the ground (Ørka et al., 2016). Our forest attribute models were consistent with those developed in comparable ecosystems with variable vegetation types in conifer dominant forests and support that while structure estimates are variable, they are consistent. For example, one recent study used lidar data to create a Norwegian forest inventory (Nilsson et al., 2017). They estimated vegetation proportions, stem density, and basal area and found a high proportion of deciduous trees can artificially increase stem densities (RMSE was ~ 10 % higher when broadleaf proportion was greater than 75 %). In post-fire temperate forests in Oregon, Zald et al. (2014) modeled basal area and stem density with an overall accuracy of $R^2 = 0.77$ and $R^2 = 0.67$ respectively. In our study, we had accuracies of $R^2 = 0.95$ and $R^2 = 0.52$ for the same two metrics. Nevertheless, improving accuracy of RPA lidar models is imperative to increase the value of our work for forest managers, who need to understand, in finer detail than our models support, the actual forest structures on the landscape (Goodbody et al., 2017).

Improving accurate and applicable quantification of structural forest recovery will rely on additional field and lidar sampling in a diversity of ecosystems and disturbance types. In a recent study using Sentinel 2 spectral data to ID bark beetle disturbances, they integrated harvester data to extrapolate the date of bark beetle attack (Jamali et al., 2023). Similarly, structural data from salvage logging operations could be used to understand the initial structural states of the forest after disturbances such as fire. Such sampling will also help to define the impact of one forest structure element (e.g., diversity in vegetation types) on another (e.g., stem counts; Saarela et al., 2015). With additional field measurements in new locations, consistent RPA models can be developed (Coops et al., 2021; Dalponte et al., 2019). These models can serve as exemplar datasets for young regenerating forests that do not have field samples. Exemplar RPA models will ultimately decrease the time investment needed for ground assessments in potentially unsafe and extensive disturbed areas (Rakochy and Hawkins, 2006; Wulder et al., 2012). Furthermore, RPA lidar collects targeted and high-density point-based structural forest data at various times after disturbance. These metrics cannot be viably collected with field-based measures. RPA Lidar also offers a distinct advantage over large area aerial Lidar acquisitions because it can produce high-density repeatable lidar assessments instead of taking years to plan, collect, and process (Frolking et al., 2009).

7. Conclusion

Monitoring forest structural recovery must prioritize identifying persistent impacts of forest disturbance and novel ecosystem developments. We present a repeatable methodology to capture variability in structural recovery by relating them to unique clusters of spectral recovery. Further, when clusters were applied to the perimeter of the Watlus Lake fire, most of the area showed strong coniferous growth. However, nearly one-tenth of areas within the fire perimeter were spatially clustered areas of lower coniferous recovery and higher deciduous growth. The spectral clusters thus identified areas that forest managers may prioritize for post-fire salvage logging, silvicultural prescriptions, or hotspots to prioritize mitigation (Rana and Vauhkonen, 2023; White et al., 2022). Landsat spectral clusters captured silviculturally valuable structural forest recovery at spatial scales previously challenging to acquire without expansive field-based structural measurements (White et al., 2023). Satellite-based analyses are cost-efficient and safety-conscious (Frolking et al., 2009). Therefore, the current study's capacity to capture variable structural recovery is pivotal for forest decision makers. Given the ability to identify variability in structural recovery in a repeatable manner, future research should capitalize on the decreasing costs of RPA lidar alongside the extension of ALS data to expand such investigations among the increasing extent of disturbed ecosystems. Expanding RPA lidar data and continued analyses on multi-index spectral trajectories will better develop the diversity of spectral trajectories and their association with variable measures of structural recovery. These spectral trajectories describe areas of low stem and basal area recovery and high deciduous ingrowth, which may be linked to novel forest structures. For those interested in future forest structure, spatially and structurally distinct pathways of forest regeneration can be highlighted using satellite-derived rates of spectral recovery.

Declaration of competing interest

The authors declare that they have no known competing financial interests or personal relationships that could have appeared to influence the work reported in this paper.

Acknowledgements

This analysis was conducted on the ancestral and unceded territories of the Dënéndeh and Tsílhqot'inNen. We thank members of these nations for the opportunity to conduct this work and for sharing their knowledge of the historic forests in casual conversation at field sites. We would also like to thank the hard work of the fieldhands: Mike Burnette and Dave Choi. This research was funded by a NSERC Alliance project Silva21 NSERC ALLRP 556265 – 20, grantee Prof. Alexis Achim.

Appendix A. Supplementary material

Supplementary data to this article can be found online at https://doi.org/10.1016/j.isprsjprs.2024.01.008.

References

Adams, J.B., Sabol, D.E., Kapos, V., Almeida Filho, R., Roberts, D.A., Smith, M.O., Gillespie, A.R., 1995. Classification of multispectral images based on fractions of endmembers: Application to land-cover change in the Brazilian Amazon. Remote Sens. Environ. 52, 137–154. https://doi.org/10.1016/0034-4257(94)00098-8.

Aggarwal, C.C., Hinneburg, A., Keim, D.A., 2001. On the Surprising Behavior of Distance Metrics in High Dimensional Space, in: Van den Bussche, J., Vianu, V. (Eds.), Database Theory — ICDT 2001, Lecture Notes in Computer Science. Springer, Berlin, Heidelberg, pp. 420–434. https://doi.org/10.1007/3-540-44503-X_27.

Baltzer, J.L., Day, N.J., Walker, X.J., Greene, D., Mack, M.C., Alexander, H.D., Arseneault, D., Barnes, J., Bergeron, Y., Boucher, Y., Bourgeau-Chavez, L., Brown, C. D., Carrière, S., Howard, B.K., Gauthier, S., Parisien, M.-A., Reid, K.A., Rogers, B.M., Roland, C., Sirois, L., Stehn, S., Thompson, D.K., Turetsky, M.R., Veraverbeke, S., Whitman, E., Yang, J., Johnstone, J.F., 2021. Increasing fire and the decline of fire adapted black spruce in the boreal forest. Proc. Natl. Acad. Sci. 118 https://doi.org/10.1073/pnas.2024872118.

Bartels, S.F., Chen, H.Y.H., Wulder, M.A., White, J.C., 2016. Trends in post-disturbance recovery rates of Canada's forests following wildfire and harvest. For. Ecol. Manage. 361, 194–207. https://doi.org/10.1016/j.foreco.2015.11.015.

BC Ministry of Forests, 2021. 2021 Burn Severity Mapping.

BC Ministry of Forests, 2023. Provincial Monitoring British Columbia.

Biodiversity Guidebook, 1995. BC Forest Practices Board.

Bolton, D.K., White, J.C., Wulder, M.A., Coops, N.C., Hermosilla, T., Yuan, X., 2018. Updating stand-level forest inventories using airborne laser scanning and Landsat time series data. Int. J. Appl. Earth Obs. Geoinf. 66, 174–183. https://doi.org/10.1016/j.jag.2017.11.016.

British Columbia Data Catalogue, 2022. Fire Perimeters - Historical [WWW Document]. URL https://catalogue.data.gov.bc.ca/dataset/fire-perimeters-historical (accessed 3.24.22).

British Columbia Ministry of Forests, 2022. Silviculture Survey Procedures Manual. Forest practices Branch, BC Ministry of Forests and Range.

Campos-Taberner, M., Javier García-Haro, F., Martínez, B., Sánchez-Ruiz, S., Moreno-Martínez, Á., Camps-Valls, G., Amparo Gilabert, M., 2023. Land use classification over smallholding areas in the European Common Agricultural Policy framework. ISPRS J. Photogramm. Remote Sens. 197, 320–334. https://doi.org/10.1016/j.isprsjprs.2023.02.005.

Chen, X., Vogelmann, J.E., Rollins, M., Ohlen, D., Key, C.H., Yang, L., Huang, C., Shi, H., 2011. Detecting post-fire burn severity and vegetation recovery using multitemporal remote sensing spectral indices and field-collected composite burn index data in a ponderosa pine forest. Int. J. Remote Sens. 32, 7905–7927. https://doi.org/10.1080/01431161.2010.524678.

Chirici, G., Giannetti, F., Mazza, E., Francini, S., Travaglini, D., Pegna, R., White, J.C., 2020. Monitoring clearcutting and subsequent rapid recovery in Mediterranean coppice forests with Landsat time series. Ann. For. Sci. 77, 1–14. https://doi.org/10.1007/s13595-020-00936-2.

Chisholm, R.A., Cui, J., Lum, S.K.Y., Chen, B.M., 2013. UAV LiDAR for below-canopy forest surveys. J. Unmanned Veh. Sys. 01, 61–68. https://doi.org/10.1139/juvs-2013-0017.

Chu, T., Guo, X., 2014. Remote sensing techniques in monitoring post-fire effects and patterns of forest recovery in boreal forest regions: a review. Remote Sens. (Basel) 6, 470–520. https://doi.org/10.3390/rs6010470.
Clason, A.J., Farnell, I., Lilles, E.B., 2022. Carbon 5–60 Years After Fire: Planting Trees Does Not Compensate for Losses in Dead Wood Stores. Frontiers in Forests and Global Change 5.
Cocke, A.E., Fulé, P.Z., Crouse, J.E., Cocke, A.E., Fulé, P.Z., Crouse, J.E., 2005. Comparison of burn severity assessments using Differenced Normalized Burn Ratio and ground data. Int. J. Wildland Fire 14, 189–198. https://doi.org/10.1071/WF04010.
Cohen, W.B., Goward, S.N., 2004. Landsat's role in ecological applications of remote sensing. Bioscience 54, 535–545. https://doi.org/10.1641/0006-3568(2004)054[0535:LRIEAO]2.0.CO;2.
Cohen, W.B., Healey, S.P., Yang, Z., Zhu, Z., Gorelick, N., 2020. Diversity of algorithm and spectral band inputs improves landsat monitoring of forest disturbance. Remote Sens. (Basel) 12, 1673. https://doi.org/10.3390/rs12101673.
Coops, N.C., Tompalski, P., Goodbody, T.R.H., Queinnec, M., Luther, J.E., Bolton, D.K., White, J.C., Wulder, M.A., van Lier, O.R., Hermosilla, T., 2021. Modelling lidar-derived estimates of forest attributes over space and time: A review of approaches and future trends. Remote Sens. Environ. 260, 112477 https://doi.org/10.1016/j.rse.2021.112477.
Crist, E.P., Cicone, R.C., 1984. A Physically-Based Transformation of Thematic Mapper Data—The TM Tasseled Cap. IEEE Transactions on Geoscience and Remote Sensing GE-22, 256–263. https://doi.org/10.1109/TGRS.1984.350619.
Czerwinski, C.J., King, D.J., Mitchell, S.W., 2014. Mapping forest growth and decline in a temperate mixed forest using temporal trend analysis of Landsat imagery, 1987–2010. Remote Sens. Environ. 141, 188–200. https://doi.org/10.1016/j.rse.2013.11.006.
Dalponte, M., Jucker, T., Liu, S., Frizzera, L., Gianelle, D., 2019. Characterizing forest carbon dynamics using multi-temporal lidar data. Remote Sens. Environ. 224, 412–420. https://doi.org/10.1016/j.rse.2019.02.018.
Davis, K.T., Dobrowski, S.Z., Higuera, P.E., Holden, Z.A., Veblen, T.T., Rother, M.T., Parks, S.A., Sala, A., Maneta, M.P., 2019. Wildfires and climate change push low-elevation forests across a critical climate threshold for tree regeneration. PNAS 116, 6193–6198. https://doi.org/10.1073/pnas.1815107116.
de Almeida, D.R.A., Stark, S.C., Valbuena, R., Broadbent, E.N., Silva, T.S.F., de Resende, A.F., Ferreira, M.P., Cardil, A., Silva, C.A., Amazonas, N., Zambrano, A.M.A., Brancalion, P.H.S., 2020. A new era in forest restoration monitoring. Restor. Ecol. 28, 8–11. https://doi.org/10.1111/rec.13067.
Dinno, A., 2017. dunn.test: Dunn's Test of Multiple Comparisons Using Rank Sums.
Donnegan, J.A., Rebertus, A.J., 1999. Rates and mechanisms of subalpine forest succession along an environmental gradient. Ecology 80, 1370–1384. https://doi.org/10.1890/0012-9658(1999)080[1370:RAMOSF]2.0.CO;2.
Dymond, C.C., Mladenoff, D.J., Radeloff, V.C., 2002. Phenological differences in Tasseled Cap indices improve deciduous forest classification. Remote Sens. Environ. 80, 460–472. https://doi.org/10.1016/S0034-4257(01)00324-8.
Epting, J., Verbyla, D., 2005. Landscape-level interactions of prefire vegetation, burn severity, and postfire vegetation over a 16-year period in interior Alaska. Can. J. for. Res. 35, 1367–1377. https://doi.org/10.1139/x05-060.
Falkowski, M.J., Evans, J.S., Martinuzzi, S., Gessler, P.E., Hudak, A.T., 2009. Characterizing forest succession with lidar data: An evaluation for the Inland Northwest, USA. Remote Sens. Environ. 113, 946–956. https://doi.org/10.1016/j.rse.2009.01.003.
Fernández-Guisuraga, J.M., Suárez-Seoane, S., Calvo, L., 2021. Radiative transfer modeling to measure fire impact and forest engineering resilience at short-term. ISPRS J. Photogramm. Remote Sens. 176, 30–41. https://doi.org/10.1016/j.isprsjprs.2021.04.002.
Fernandez-Manso, A., Quintano, C., Roberts, D.A., 2016. Burn severity influence on post-fire vegetation cover resilience from Landsat MESMA fraction images time series in Mediterranean forest ecosystems. Remote Sens. Environ. 184, 112–123. https://doi.org/10.1016/j.rse.2016.06.015.
Fornacca, D., Ren, G., Xiao, W., 2018. Evaluating the best spectral indices for the detection of burn scars at several post-fire dates in a mountainous Region of Northwest Yunnan. China. Remote Sensing 10, 1196. https://doi.org/10.3390/rs10081196.
Frolking, S., Palace, M.W., Clark, D.B., Chambers, J.Q., Shugart, H.H., Hurtt, G.C., 2009. Forest disturbance and recovery: A general review in the context of spaceborne remote sensing of impacts on aboveground biomass and canopy structure. J. Geophys. Res.-Biogeosci. 114, G00E02. https://doi.org/10.1029/2008JG000911.
Gómez, C., White, J.C., Wulder, M.A., Alejandro, P., 2014. Historical forest biomass dynamics modelled with Landsat spectral trajectories. ISPRS J. Photogramm. Remote Sens. 93, 14–28. https://doi.org/10.1016/j.isprsjprs.2014.03.008.
Goodbody, T.R.H., Coops, N.C., Marshall, P.L., Tompalski, P., Crawford, P., 2017. Unmanned aerial systems for precision forest inventory purposes: A review and case study. For. Chron. 93, 71–81. https://doi.org/10.5558/tfc2017-012.
Hansen, W.D., Turner, M.G., 2019. Origins of abrupt change? Postfire subalpine conifer regeneration declines nonlinearly with warming and drying. Ecol. Monogr. 89, e01340.
Harvey, B.J., Andrus, R.A., Anderson, S.C., 2019. Incorporating biophysical gradients and uncertainty into burn severity maps in a temperate fire-prone forested region. Ecosphere 10, e02600.
Hayes, K., Buma, B., 2021. Effects of short-interval disturbances continue to accumulate, overwhelming variability in local resilience. Ecosphere 12, e03379.
Hennig, C., 2020. fpc: Flexible Procedures for Clustering.
Hermosilla, T., Wulder, M.A., White, J.C., Coops, N.C., Hobart, G.W., 2015. Regional detection, characterization, and attribution of annual forest change from 1984 to 2012 using Landsat-derived time-series metrics. Remote Sens. Environ. 170, 121–132. https://doi.org/10.1016/j.rse.2015.09.004.
Hermosilla, T., Wulder, M.A., White, J.C., Coops, N.C., Hobart, G.W., Campbell, L.B., 2016. Mass data processing of time series Landsat imagery: pixels to data products for forest monitoring. Int. J. Digital Earth 9, 1035–1054. https://doi.org/10.1080/17538947.2016.1187673.
Hermosilla, T., Wulder, M.A., White, J.C., Coops, N.C., Hobart, G.W., 2018. Disturbance-Informed Annual Land Cover Classification Maps of Canada's Forested Ecosystems for a 29-Year Landsat Time Series. Can. J. Remote. Sens. 44, 67–87. https://doi.org/10.1080/07038992.2018.1437719.
Hessburg, P.F., Agee, J.K., Franklin, J.F., 2005. Dry forests and wildland fires of the inland Northwest USA: Contrasting the landscape ecology of the pre-settlement and modern eras. Forest Ecology and Management, Relative Risk Assessments for Decision –Making Related To Uncharacteristic Wildfire 211, 117–139. https://doi.org/10.1016/j.foreco.2005.02.016.
Hesselbarth, M.H.K., Sciaini, M., With, K.A., Wiegand, K., Nowosad, J., 2019. landscapemetrics: an open-source R tool to calculate landscape metrics. Ecography 42, 1648–1657.
Horler, D.N.H., Ahern, F.J., 1986. Forestry information content of Thematic Mapper data. Int. J. Remote Sens. 7, 405–428. https://doi.org/10.1080/01431168608954695.
Huang, S., Ramirez, C., McElhaney, M., Clark, C., Yao, Z., 2019. Quantifying spatiotemporal post-disturbance recovery using field inventory, tree growth, and remote sensing. Earth Space Sci. 6, 489–504. https://doi.org/10.1029/2018EA000489.
Isenburg, M., 2014. LAStools, "Efficient LiDAR Processing Software.".
Jamali, S., Olsson, P.-O., Ghorbanian, A., Müller, M., 2023. Examining the potential for early detection of spruce bark beetle attacks using multi-temporal Sentinel-2 and harvester data. ISPRS J. Photogramm. Remote Sens. 205, 352–366. https://doi.org/10.1016/j.isprsjprs.2023.10.013.
Jarron, L.R., Coops, N.C., MacKenzie, W.H., Tompalski, P., Dykstra, P., 2020. Detection of sub-canopy forest structure using airborne LiDAR. Remote Sens. Environ. 244, 111770 https://doi.org/10.1016/j.rse.2020.111770.
Karvanen, J., 2006. Estimation of quantile mixtures via L-moments and trimmed L-moments. Comput. Stat. Data Anal. 51, 947–959. https://doi.org/10.1016/j.csda.2005.09.014.
Keeley, J.E., 2009. Fire intensity, fire severity and burn severity: a brief review and suggested usage. Int. J. Wildland Fire 18, 116–126. https://doi.org/10.1071/WF07049.
Key, C.H., Benson, N.C., 2006. Landscape Assessment (LA).
Kiel, N.G., Turner, M.G., 2022. Where are the trees? Extent, configuration, and drivers of poor forest recovery 30 years after the 1988 Yellowstone fires. For. Ecol. Manage. 524, 120536 https://doi.org/10.1016/j.foreco.2022.120536.
Klápště, P., Fogl, M., Barták, V., Gdulová, K., Urban, R., Moudrý, V., 2020. Sensitivity analysis of parameters and contrasting performance of ground filtering algorithms with UAV photogrammetry-based and LiDAR point clouds. Int. J. Digital Earth 13, 1672–1694. https://doi.org/10.1080/17538947.2020.1791267.
Lewis, S.A., Hudak, A.T., Robichaud, P.R., Morgan, P., Satterberg, K.L., Strand, E.K., Smith, A.M.S., Zamudio, J.A., Lentile, L.B., Lewis, S.A., Hudak, A.T., Robichaud, P.R., Morgan, P., Satterberg, K.L., Strand, E.K., Smith, A.M.S., Zamudio, J.A., Lentile, L.B., 2017. Indicators of burn severity at extended temporal scales: a decade of ecosystem response in mixed-conifer forests of western Montana. Int. J. Wildland Fire 26, 755–771. https://doi.org/10.1071/WF17019.
Meidinger, D.V., Pojar, J., 1991. Ecosystems of British Columbia. B.C, Ministry of Forests.
Millar, C.I., Stephenson, N.L., 2015. Temperate forest health in an era of emerging megadisturbance. Science 349, 823–826. https://doi.org/10.1126/science.aaa9933.
Miller, J.D., Thode, A.E., 2007. Quantifying burn severity in a heterogeneous landscape with a relative version of the delta Normalized Burn Ratio (dNBR). Remote Sens. Environ. 109, 66–80. https://doi.org/10.1016/j.rse.2006.12.006.
Moe, K.T., Owari, T., Furuya, N., Hiroshima, T., 2020. Comparing Individual Tree Height Information Derived from Field Surveys, LiDAR and UAV-DAP for High-Value Timber Species in Northern Japan. Forests 11, 223. https://doi.org/10.3390/f11020223.
Moreno-Fernández, D., Viana-Soto, A., Camarero, J.J., Zavala, M.A., Tijerín, J., García, M., 2021. Using spectral indices as early warning signals of forest dieback: The case of drought-prone Pinus pinaster forests. Sci. Total Environ. 793, 148578 https://doi.org/10.1016/j.scitotenv.2021.148578.
Morresi, D., Vitali, A., Urbinati, C., Garbarino, M., 2019. Forest spectral recovery and regeneration dynamics in stand-replacing wildfires of central Apennines derived from Landsat time series. Remote Sens. (Basel) 11, 308. https://doi.org/10.3390/rs11030308.
Nguyen, T.H., Jones, S.D., Soto-Berelov, M., Haywood, A., Hislop, S., 2018. A spatial and temporal analysis of forest dynamics using Landsat time-series. Remote Sens. Environ. 217, 461–475. https://doi.org/10.1016/j.rse.2018.08.028.
Nguyen, T.H., Jones, S., Soto-Berelov, M., Haywood, A., Hislop, S., 2020. Landsat time-series for estimating forest aboveground biomass and its dynamics across space and time: a review. Remote Sens. (Basel) 12, 98. https://doi.org/10.3390/rs12010098.
Nilson, T., Peterson, U., 1994. Age dependence of forest reflectance: Analysis of main driving factors. Remote Sens. Environ. 48, 319–331. https://doi.org/10.1016/0034-4257(94)90006-X.
Nilsson, M., Nordkvist, K., Jonzén, J., Lindgren, N., Axensten, P., Wallerman, J., Egberth, M., Larsson, S., Nilsson, L., Eriksson, J., Olsson, H., 2017. A nationwide forest attribute map of Sweden predicted using airborne laser scanning data and field data from the National Forest Inventory. Remote Sens. Environ. 194, 447–454. https://doi.org/10.1016/j.rse.2016.10.022.
Ogle, D.H., Doll, J.C., Wheeler, P., Dinno, A., 2022. FSA: Fisheries Stock Analysis.

Ørka, H.O., Gobakken, T., Næsset, E., 2016. Predicting attributes of regeneration forests using airborne laser scanning. Can. J. Remote. Sens. 42, 541–553. https://doi.org/10.1080/07038992.2016.1199269.
Pajares, G., 2015. Overview and Current Status of Remote Sensing Applications Based on Unmanned Aerial Vehicles (UAVs) [WWW Document]. https://doi.org/info:doi/10.14358/PERS.81.4.281.
Pasquarella, V.J., Holden, C.E., Kaufman, L., Woodcock, C.E., 2016. From imagery to ecology: leveraging time series of all available Landsat observations to map and monitor ecosystem state and dynamics. Remote Sens. Ecol. Conserv. 2, 152–170. https://doi.org/10.1002/rse2.24.
Pausas, J.G., Keeley, J.E., 2021. Wildfires and global change. Front. Ecol. Environ. 19, 387–395. https://doi.org/10.1002/fee.2359.
Peterson, U., 1992. Seasonal reflectance factor dynamics in boreal forest clear-cut communities. Int. J. Remote Sens. 13, 753–772. https://doi.org/10.1080/01431169208904150.
Pflugmacher, D., Cohen, W.B., E. Kennedy, R., 2012. Using Landsat-derived disturbance history (1972–2010) to predict current forest structure. Remote Sensing of Environment, Landsat Legacy Special Issue 122, 146–165. https://doi.org/10.1016/j.rse.2011.09.025.
Pickell, P.D., Hermosilla, T., Frazier, R.J., Coops, N.C., Wulder, M.A., 2016. Forest recovery trends derived from Landsat time series for North American boreal forests. Int. J. Remote Sens. 37, 138–149. https://doi.org/10.1080/2150704X.2015.1126375.
Rakochy, P., Hawkins, C., 2006. Wildlife/danger tree assessment in unharvested stands attacked by mountain pine beetle in the central interior of British Columbia. J. Ecosyst. Manage. 7.
Rana, P., Vauhkonen, J., 2023. Stochastic multicriteria acceptability analysis as a forest management priority mapping approach based on airborne laser scanning and field inventory data. Landsc. Urban Plan. 230, 104637 https://doi.org/10.1016/j.landurbplan.2022.104637.
Richards, J.A., Jia, X. (Eds.), 2006. Clustering and Unsupervised Classification, in: Remote Sensing Digital Image Analysis: An Introduction. Springer, Berlin, Heidelberg, pp. 249–266. https://doi.org/10.1007/3-540-29711-1_9.
Roussel, J.-R., Auty, D., Coops, N.C., Tompalski, P., Goodbody, T.R.H., Meador, A.S., Bourdon, J.-F., de Boissieu, F., Achim, A., 2020. lidR: An R package for analysis of Airborne Laser Scanning (ALS) data. Remote Sens. Environ. 251, 112061 https://doi.org/10.1016/j.rse.2020.112061.
Saarela, S., Grafström, A., Ståhl, G., Kangas, A., Holopainen, M., Tuominen, S., Nordkvist, K., Hyyppä, J., 2015. Model-assisted estimation of growing stock volume using different combinations of LiDAR and Landsat data as auxiliary information. Remote Sens. Environ. 158, 431–440. https://doi.org/10.1016/j.rse.2014.11.020.
Saverio, F., 2021. BAP-GEE.
Seidl, R., Turner, M.G., 2022. Post-disturbance reorganization of forest ecosystems in a changing world. Proc. Natl. Acad. Sci. 119 https://doi.org/10.1073/pnas.2202190119.
Senf, C., Müller, J., Seidl, R., 2019. Post-disturbance recovery of forest cover and tree height differ with management in Central Europe. Landscape Ecol 34, 2837–2850. https://doi.org/10.1007/s10980-019-00921-9.
Senf, C., Seidl, R., 2022. Post-disturbance canopy recovery and the resilience of Europe's forests. Glob. Ecol. Biogeogr. 31, 25–36. https://doi.org/10.1111/geb.13406.
Shrestha, M., Broadbent, E.N., Vogel, J.G., 2021. Using GatorEye UAV-borne LiDAR to quantify the spatial and temporal effects of a prescribed fire on understory height and biomass in a pine savanna. Forests 12, 38. https://doi.org/10.3390/f12010038.
Solans Vila, J.P., Barbosa, P., 2010. Post-fire vegetation regrowth detection in the Deiva Marina region (Liguria-Italy) using Landsat TM and ETM+ data. Ecological Modelling, Special Issue on Spatial and Temporal Patterns of Wildfires: Models, Theory, and Reality 221, 75–84. https://doi.org/10.1016/j.ecolmodel.2009.03.011.
Steen, O.A., Coupé, R.A., 1997. A field guide to forest site identification and interpretation for the Cariboo Forest Region. Land management handbook, British Columbia, Ministry of Forests, Research Program, Victoria, BC.
Stevens-Rumann, C.S., Morgan, P., 2019. Tree regeneration following wildfires in the western US: a review. Fire Ecol. 15, UNSP 15. https://doi.org/10.1186/s42408-019-0032-1.
Talucci, A.C., Lertzman, K.P., Krawchuk, M.A., 2019. Drivers of lodgepole pine recruitment across a gradient of bark beetle outbreak and wildfire in British Columbia. For. Ecol. Manage. 451, 117500 https://doi.org/10.1016/j.foreco.2019.117500.
van Ewijk, K.Y., Treitz, P.M., Scott, N.A., 2011. Characterizing forest succession in central Ontario using Lidar-derived indices. Photogramm. Eng. Remote Sens. 77, 261–269. https://doi.org/10.14358/PERS.77.3.261.
Vanderhoof, M., Hawbaker, T., 2018. It matters when you measure it: using snow-cover normalised difference vegetation index (NDVI) to isolate post-fire conifer regeneration. Int. J. Wildland Fire 27. https://doi.org/10.1071/WF18075.
Viana-Soto, A., Aguado, I., Salas, J., García, M., 2020. Identifying post-fire recovery trajectories and driving factors using Landsat time series in fire-prone Mediterranean pine forests. Remote Sens. (Basel) 12, 1499. https://doi.org/10.3390/rs12091499.
Waldron, K., Thiffault, N., Venier, L., Bognounou, F., Boucher, D., Campbell, E., Whitman, E., Brehaut, L., Gauthier, S., 2023. A pan-Canadian assessment of empirical research on post-disturbance recovery in the Canadian Forest Service. Can. J. for. Res. 53, 823–838. https://doi.org/10.1139/cjfr-2022-0300.
Westerling, A.L., Hidalgo, H.G., Cayan, D.R., Swetnam, T.W., 2006. Warming and earlier spring increase western U.S. Forest Wildfire Activity. Science 313, 940–943. https://doi.org/10.1126/science.1128834.
White, J. C., Tompalski, P., Vastaranta, M., Wulder, M.A., Saarinen, N., Stepper, C., Coops, N.C., 2017. A model development and application guide for generating an enhanced forest inventory using airborne laser scanning data and an area-based approach.
White, J.C., Wulder, M.A., Hobart, G.W., Luther, J.E., Hermosilla, T., Griffiths, P., Coops, N.C., Hall, R.J., Hostert, P., Dyk, A., Guindon, L., 2014. Pixel-based image compositing for large-area dense time series applications and science. Can. J. Remote. Sens. 40, 192–212. https://doi.org/10.1080/07038992.2014.945827.
White, J.C., Wulder, M.A., Hermosilla, T., Coops, N.C., Hobart, G.W., 2017b. A nationwide annual characterization of 25years of forest disturbance and recovery for Canada using Landsat time series. Remote Sens. Environ. 194, 303–321. https://doi.org/10.1016/j.rse.2017.03.035.
White, J.C., Saarinen, N., Kankare, V., Wulder, M.A., Hermosilla, T., Coops, N.C., Pickell, P.D., Holopainen, M., Hyyppä, J., Vastaranta, M., 2018. Confirmation of post-harvest spectral recovery from Landsat time series using measures of forest cover and height derived from airborne laser scanning data. Remote Sens. Environ. 216, 262–275. https://doi.org/10.1016/j.rse.2018.07.004.
White, J.C., Hermosilla, T., Wulder, M.A., Coops, N.C., 2022. Mapping, validating, and interpreting spatio-temporal trends in post-disturbance forest recovery. Remote Sens. Environ. 271, 112904 https://doi.org/10.1016/j.rse.2022.112904.
White, J.C., Hermosilla, T., Wulder, M.A., 2023. Pre-fire measures of boreal forest structure and composition inform interpretation of post-fire spectral recovery rates. For. Ecol. Manage. 537, 120948 https://doi.org/10.1016/j.foreco.2023.120948.
Williamson, T.B., Johnston, M.H., Nelson, H.W., Edwards, J.E., 2019. Adapting to climate change in Canadian forest management: past, present and future. For. Chron. 95, 76–90. https://doi.org/10.5558/tfc2019-015.
Wulder, M.A., White, J.C., Alvarez, F., Han, T., Rogan, J., Hawkes, B., 2009. Characterizing boreal forest wildfire with multi-temporal Landsat and LIDAR data. Remote Sens. Environ. Monit. Protected Areas 113, 1540–1555. https://doi.org/10.1016/j.rse.2009.03.004.
Wulder, M.A., White, J.C., Bater, C.W., Coops, N.C., Hopkinson, C., Chen, G., 2012. Lidar plots — a new large-area data collection option: context, concepts, and case study. Can. J. Remote. Sens. 38, 600–618. https://doi.org/10.5589/m12-049.
Wulder, M.A., Roy, D.P., Radeloff, V.C., Loveland, T.R., Anderson, M.C., Johnson, D.M., Healey, S., Zhu, Z., Scambos, T.A., Pahlevan, N., Hansen, M., Gorelick, N., Crawford, C.J., Masek, J.G., Hermosilla, T., White, J.C., Belward, A.S., Schaaf, C., Woodcock, C.E., Huntington, J.L., Lymburner, L., Hostert, P., Gao, F., Lyapustin, A., Pekel, J.-F., Strobl, P., Cook, B.D., 2022. Fifty years of Landsat science and impacts. Remote Sens. Environ. 280, 113195 https://doi.org/10.1016/j.rse.2022.113195.
Young, N.E., Anderson, R.S., Chignell, S.M., Vorster, A.G., Lawrence, R., Evangelista, P. H., 2017. A survival guide to Landsat preprocessing. Ecology 98, 920–932. https://doi.org/10.1002/ecy.1730.
Zald, H.S.J., Ohmann, J.L., Roberts, H.M., Gregory, M.J., Henderson, E.B., McGaughey, R.J., Braaten, J., 2014. Influence of lidar, Landsat imagery, disturbance history, plot location accuracy, and plot size on accuracy of imputation maps of forest composition and structure. Remote Sens. Environ. 143, 26–38. https://doi.org/10.1016/j.rse.2013.12.013.
Zhu, Z., Zhang, J., Yang, Z., Aljaddani, A.H., Cohen, W.B., Qiu, S., Zhou, C., 2020. Continuous monitoring of land disturbance based on Landsat time series. Remote Sensing of Environment, Time Series Analysis with High Spatial Resolution Imagery 238, 111116. https://doi.org/10.1016/j.rse.2019.03.009.